NAVAL POSTGRADUATE SCHOOL
Monterey, California

THESIS

A FEASABILITY STUDY OF
OCEAN ACOUSTIC TOMOGRAPHY
IN THE BARENTS SEA

by

John Mark Emblidge

September, 1991

Thesis Advisor:	Ching-Sang Chiu
Co-Advisor	James H. Miller
Co-Advisor	Robert H. Bourke

Unclassified

Security Classification of this page

REPORT DOCUMENTATION PAGE

1a Report Security Classification: Unclassified	1b Restrictive Markings
2a Security Classification Authority	3 Distribution Availability of Report: Approved for public release; distribution is unlimited
2b Declassification/Downgrading Schedule	
4 Performing Organization Report Number(s)	5 Monitoring Organization Report Number(s)
6a Name of Performing Organization: Naval Postgraduate School; 6b Office Symbol (*If Applicable*): 35	7a Name of Monitoring Organization: Naval Postgraduate School
6c Address (*city, state, and ZIP code*): Monterey, CA 93943-5000	7b Address (*city, state, and ZIP code*): Monterey, CA 93943-5000
8a Name of Funding/Sponsoring Organization; 8b Office Symbol (*If Applicable*)	9 Procurement Instrument Identification Number
8c Address (*city, state, and ZIP code*)	10 Source of Funding Numbers: Program Element Number; Project No; Task No; Work Unit Accession No

11 Title (*Include Security Classification*): A FEASIBILITY STUDY OF OCEAN ACOUSTIC TOMOGRAPHY IN THE BARENTS SEA

12 Personal Author(s): Emblidge, John M.

13a Type of Report	13b Time Covered	14 Date of Report (*year, month,day*)	15 Page Count
Master's Thesis	From To	September 1991	93

16 Supplementary Notation: The views expressed in this thesis are those of the author and do not reflect the official policy or position of the Department of Defense or the U.S. Government.

17 Cosati Codes			18 Subject Terms (*continue on reverse if necessary and identify by block number*)
Field	Group	Subgroup	Acoustic Tomography, Ocean Acoustics, Oceanography, Barents Sea

19 Abstract (*continue on reverse if necessary and identify by block number*)

The purpose of this thesis is to explore the feasibility of conducting vertical array ocean acoustic tomography in the Barents Sea. This effort is in support of the Barents Sea Acoustic Tomography Transmission Test experiment to be carried out in the summer of 1992 by NPS and Woods Hole Oceanographic Institution (WHOI). This study is conducted in two stages: a literature search and a computer simulation of acoustic ray propagation in the Barents Sea.

The literature search gathered oceanographic, geophysical, and climatological data on the Barents Sea. These data were used to form a picture of the oceanographic conditions expected to exist in the Barents Sea in August and to estimate the acoustic bottom, surface and scattering losses that the tomographic signal could be subjected to. Also the noise levels in the Barents Sea were determined from these data.

The computer simulation of tomographic transmission in the Barents Sea was conducted using HARPO (Hamiltonian Acoustic Raytracing Program for the Ocean). This program provided raytraces for acoustic rays launched between 0° and 25° from one of the three planned sources to the receiver array. This analysis determined that tomography in the Barents Sea is possible, and that the planned source level of the sources will be large enough to overcome the environmental losses.

20 Distribution/Availability of Abstract	21 Abstract Security Classification
[X] unclassified/unlimited [ ] same as report [ ] DTIC users	Unclassified

22a Name of Responsible Individual	22b Telephone (*Include Area code*)	22c Office Symbol
Dr. Ching-Sang Chiu	(408) 646-3239	OC/Ci

DD FORM 1473, JUN 86 *Previous editions are obselete.* S/N 0102-LF-014-6603

SECURITY CLASSIFICATION OF THIS PAGE
Unclassified

Approved for public release; distribution is unlimited.

A Feasibility Study of
Ocean Acoustic Tomography
in the Barents Sea

by

John Mark Emblidge
Lieutenant, U.S. Navy
B.A. Alfred University, 1984

Submitted in partial fulfillment of the requirements for
the degree of

MASTER OF SCIENCE IN PHYSICAL OCEANOGRAPHY

from the

NAVAL POSTGRADUATE SCHOOL
September 1991

Author: _____
John M. Emblidge

Approved by: _____
Ching-Sang Chiu, Thesis Advisor

_____
James H. Miller, Thesis Co-Advisor

_____
Robert H. Bourke, Thesis Co-Advisor

_____
Curtis A. Collins
Chairman, Department of Oceanography

ABSTRACT

The purpose of this thesis is to explore the feasibility of conducting vertical array ocean acoustic tomography in the Barents Sea. This effort is in support of the Barents Sea Acoustic Tomography Transmission Test experiment to be carried out in the summer of 1992 by NPS and Woods Hole Oceanographic Institution (WHOI). This study is conducted in two stages: a literature search and a computer simulation of acoustic ray propagation in the Barents Sea.

The literature search gathered oceanographic, geophysical, and climatological data on the Barents Sea. These data were used to form a picture of the oceanographic conditions expected to exist in the Barents Sea in August and to estimate the acoustic bottom, surface and scattering losses that the tomographic signal could be subjected to. Also the noise levels in the Barents Sea were determined from these data.

The computer simulation of tomographic transmission in the Barents Sea was conducted using HARPO (Hamiltonian Acoustic Ray tracing Program for the Ocean). This program provided raytraces for acoustic rays launched between 0° and 25° from one of the three planned sources to the receiver array. This analysis determined that tomography in the Barents Sea is possible, and that the planned source level of the sources will be large enough to overcome the environmental losses.

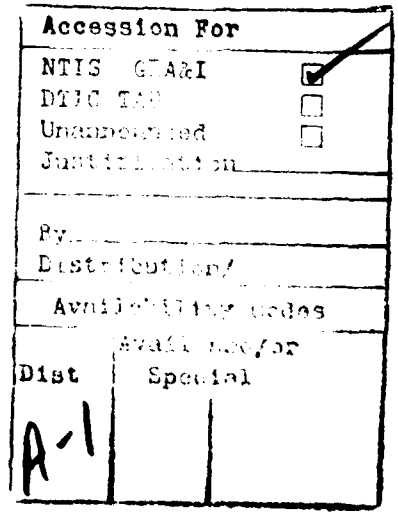

TABLE OF CONTENTS

Figures List

Table List

I. INTRODUCTION

A. Ocean Acoustic Tomography

The technique of tomography is one in which an unknown structure's interior is examined using exterior sensors. Examples are electro-magnetic (E-M), seismic, or sound waves which can propagate through media that are transparent to them and can reveal a wealth of information to the investigator if the proper mathematical techniques are applied. Medical science has long used X-rays for Computer Assisted Tomography (CAT), and geophysists probe the Earth's interior with natural and manmade seismic waves (Backus, and Gilbert, 1967). Application of these techniques to the ocean was first proposed by Munk and Wunsch (1977) as a means for monitoring mesoscale fluctuations in ocean basins. Measurements of perturbation travel times of sound pulses traveling between multiple sources and receivers contain a great deal of information about the ocean surrounded by the sensors.

Ocean acoustic tomography has several advantages over more traditional oceanographic study methods (Chiu *et al.*, 1987). A tomographic monitoring system can be installed as a semipermanent, continuous, weather-independent observing system. The low spatial attenuation rate of sound allows the system to monitor large volumes of the ocean with relatively

few acoustic moorings, and consequently much lower cost than traditional systems. Furthermore, with traditional moorings each additional mooring adds only one new piece of information such that a 1:1 mooring increase to information gain ratio occurs. In contrast the addition of one tomographic mooring adds many new and distinct ray paths each of which adds a piece of information to the system (Munk and Wunsch, 1979).

An ocean acoustic tomography exercise can be partitioned into two separate and distinct parts. The first is known as the "*forward*" problem and the second as the "*inverse*" problem (Munk and Wunsch, 1979). The forward problem establishes the physical relationship between data and the unknown structure. Simulation studies using this established relationship can be used to investigate signal design issues. Within the context of ray acoustics the forward problem can be formulated as a Fredholm Integral of the First Kind as follows:

$$\delta t_i = \int \frac{-1}{c^2(s_i)} \delta c(s_i)\, ds_i + e_i \qquad i = 1,2,\ldots n \quad \text{Eq. 1.1}$$

where δt_i is the travel time change observed from the i^{th} acoustic ray path (s_i), $-1/c^2(s_i)$ is the data kernel expressing the physical relation between the unknown medium and the data, c is the known reference sound speed field, δc is the unknown perturbation of sound speed to be estimated, and e_i is the measurement noise.

The signal design problem has five important issues which determine if the data gathered are useful:

1. Stability
2. Resolvability
3. Identifiability
4. Oceanographic signal strength
5. Signal to noise ratio (SNR)

Stability addresses the property of whether or not the same individual arrival exists over successive transmissions. Stability requires that the eigenray[1] paths be insensitive to changes in the medium. Resolvability requires that the temporal separation of eigenray arrivals be large enough to resolve individual rays. The third issue, identifiability, requires that the measured arrival times of the eigenrays match the modeled arrive times so that one knows the association of arrivals to raypaths (Spindel, 1986). The strength of oceanographic signals determine the observability of particular ocean processes in the travel times and SNR determines the limiting range of transmission. These two issues will be discussed in detail in later chapters.

Once the forward problem has been posed and the data gathered, the unknown structure can be reconstructed using inverse methods. These methods generally find a suite of solutions for the unknown structure all of which are consistent with the data gathered. There are many possible

[1]Eigenrays are rays that directly connect a particular source to a particular receiver.

solutions to the same inverse problem because it is an underdetermined problem (all ocean acoustic tomography problems are ill posed). The best solution can be chosen from the many possible solutions based on some objective criteria (Parker, 1977). The inverse problem is not dealt with in this thesis. A complete description of linear inverse theory may be found in a number of sources including Parker (1977), Backus and Gilbert (1967), and Wiggins (1972).

B. Barents Sea Acoustic Tomography Transmission Test

The Barents Sea Acoustic Tomography Transmission Test (BATT) is planned to be conducted in August 1992. The test tomography system will include two transceiver moorings, one source mooring and one bottom moored vertical array, 240 m in length, composed of 12 equally spaced receivers. Figure 1.1 shows the proposed experimental configuration, the details of the bathymetry, and the probable location of the core of the Barents Sea Polar Front. The characteristics of the sources and receivers are displayed in Table 1.1. The test will be conducted as a joint effort between Woods Hole Oceanographic Institution (WHOI) and the Naval Postgraduate School (NPS), with possible additional contributions from various Russian laboratories.

The scientific objectives of this test can be summarized as follows (Chiu, 1991a):

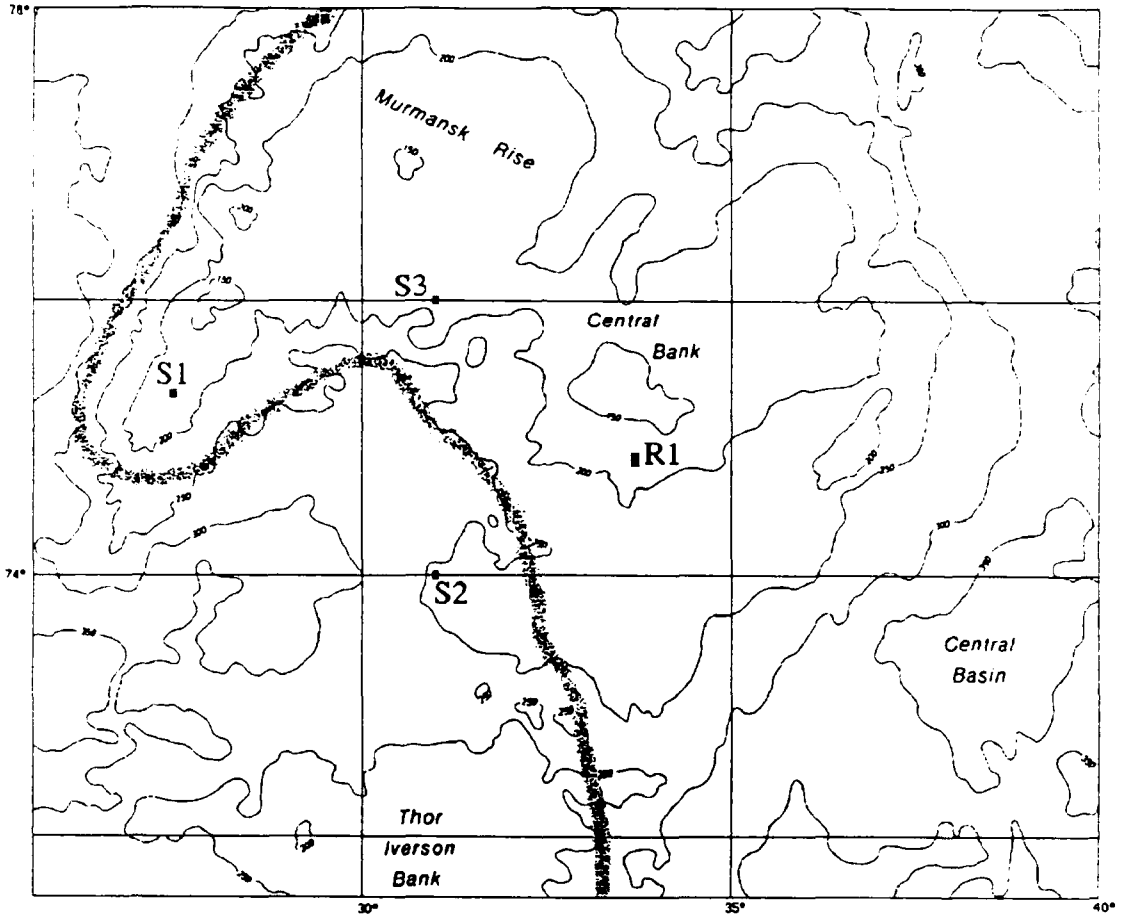

Figure 1.1 Locations of the sources(S) and the receiver(R) array and the mean frontal position. Contour interval 50m (Cherkis *et al.*,1990).

1. Determine the feasibility of monitoring circulation in the Barents Sea region using vertical-hydrophone-array tomography.

2. Examine the vertical-temporal coherence of the acoustic wavefield.

3. Map and study frontal oscillations using ray/mode inverse techniques.

TABLE 1.1 Locations and Characteristics of Acoustic Elements.

	Latitude	Longitude	Type	Freq (Hz)	Band-width (Hz)
S1	74.45°N	34.4°E	Transceiver	400	100
S2	74.00°N	36.00°E	Source	224,250	16,100
S3	75.00°N	36.00°E	Transceiver	400	100
R1	74.20°N	38.70°E	Receiver Array	N/A	N/A

C. Thesis Objectives and Approaches

The two basic objectives of this thesis are set forth here. The first is to study the oceanographic, geophysical, and climatological conditions of the Barents Sea to gain a better understanding of the environment. This is achieved through a literature search and personal contacts with various scientists. The second objective is to address the tomography issues discussed previously by examining the expected arrival structure of acoustic rays.

The approach used to achieve the second objective is to use the ray tracing program HARPO (Hamiltonian Acoustic Raytracing Program for the Ocean) with simulated conditions anticipated during the BATT. The environmental information gathered provided the basis for building a "mathematical" ocean used by HARPO to trace acoustic rays from a source to the receiving array. Use of actual CTD data for synthesis of the sound speed fields will permit the modeled ocean to more

closely approximate actual conditions than might otherwise be possible.

The oceanographic signal strength will be examined by looking at the results of various HARPO runs. By plotting travel time against launch angle for the three different frontal situations modeled as discussed in Chapter IV. The signal-to-noise-ratio (SNR) will be examined using parameters calculated by HARPO (spreading loss, and absorption) and adding in the bottom and surface losses and environmental noise effects that are calculated in Chapter III.

D. Thesis Outline

The remainder of this thesis consists of four chapters. Chapter II describes the physical oceanography of the Barents Sea including currents, water masses, and Polar Front features. Also included are discussions of the bathymetry and geologic processes which created the bathymetry, and finally a discussion of climatology.

Chapter III dwells on the acoustic properties of the Barents Sea. Here bottom loss, surface loss, and the sonar equation are explored and calculations of signal-to-noise ratio (SNR) conducted.

In Chapter IV a brief review of ray theory and of the ray tracing program, HARPO, is presented. The discussion dwells upon the basics of ray theory and the modeling of the Barents Sea for HARPO. Also the results of the numerous HARPO runs

and the travel time and arrival structure differences that result from varying the position of the Barents Sea Polar Front are presented. Based upon these results the issues of acoustic signal stability, resolvability, and travel time change due to frontal oscillation are examined.

Chapter V presents the conclusion of this study.

II. PHYSICAL OCEANOGRAPHY

A. INTRODUCTION

The Barents Sea, named for Dutch explorer Willem Barents, is a platform type sea[2] which covers the westernmost portion of the Eurasian shelf (Klenova, 1966). The Barents Sea is bordered to the south by the coasts of Scandinavia and the Russian Republic, to the north by the Svalbard Archipelago, Franz Joseph Land, and other islands along the southern edge of the Arctic Ocean. It is bounded on the eastern side by Novaya Zemlya. Its western boundary is open but can be approximated by the 15°E meridian (Figure 2.1). With an average depth of only 230 m and a maximum depth of 500 m, the Barents Sea is among the shallowest seas of the world ocean (Klenova, 1966). This shallow bottom results in hydrographic characteristics that are largely controlled by the underlying topography.

The geographical location of the Barents Sea also leads to the presence of complex oceanographic structures. The confluence of Polar and Atlantic water masses to the east of Bear Island forms the Barents Sea Polar Front which varies in intensity across most of the sea. The incursion of warm

[2] A platform sea is one whose floor is raised up, as on a platform, from the surrounding basins (Klenova, 1966).

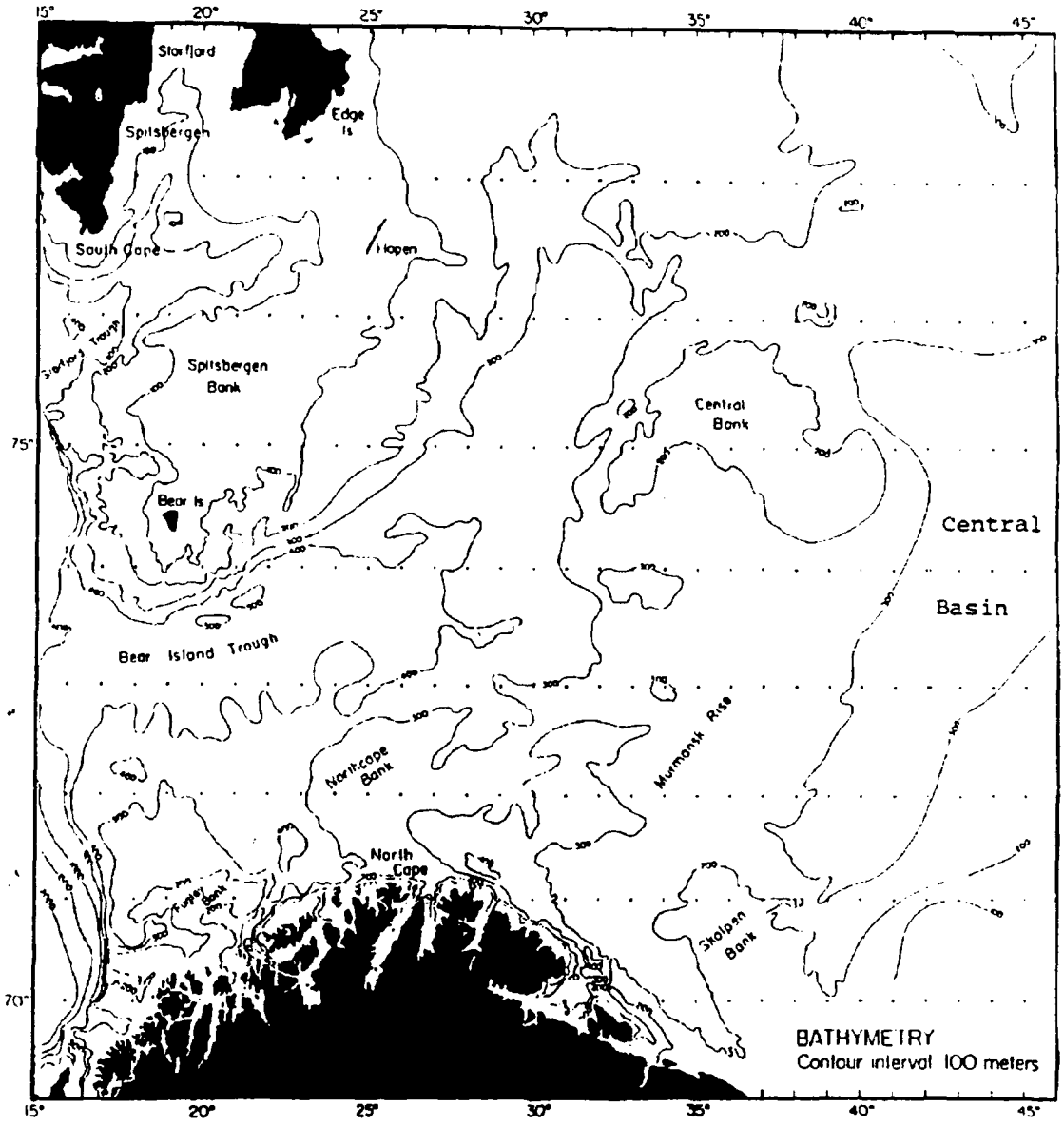

Figure 2.1 Bathymetric chart of the Barents Sea (after Eldholm and Talwani, 1977).

Atlantic Water into this Arctic sea leads to relatively mild climatic conditions in the Barents Sea, discussed later, and allows at least part of the sea to be navigable year round (Loeng and Vinje, 1979).

The 1992 Barents Sea Acoustic Tomography Transmission Test will be conducted in the region surrounding the Central Bank (Figure 2.1). The emphasis of this chapter will be on the oceanographic conditions expected to exist in the Central Bank region during the proposed time frame of the transmission test (August and September). However, considerable discussion of other regions of the Barents Sea will be included for completeness.

This discussion will focus on how the bottom, the surface, and the water masses (i.e., sound speed profiles) are expected to affect the propagation of low frequency sound. Another important factor is sea ice. However, the maximum southward extent of sea ice at the end of August is approximately 77°N (approximately 180 km to the north of the experiment location) while the minimum extent is well north of Spitsbergen and Franz Joseph Land (Midttun, and Loeng, 1987) (Figure 2.2). Thus, the likelihood of sea ice being present near the Central Bank in August is negligible and will not be considered here. We will, however, consider the impact of ambient noise radiated by the ice edge on array performance in Chapter III. The climatology of the Barents Sea and how it may affect the conduct of the experiment is also of concern. We will pay particular attention to navigation and station keeping issues.

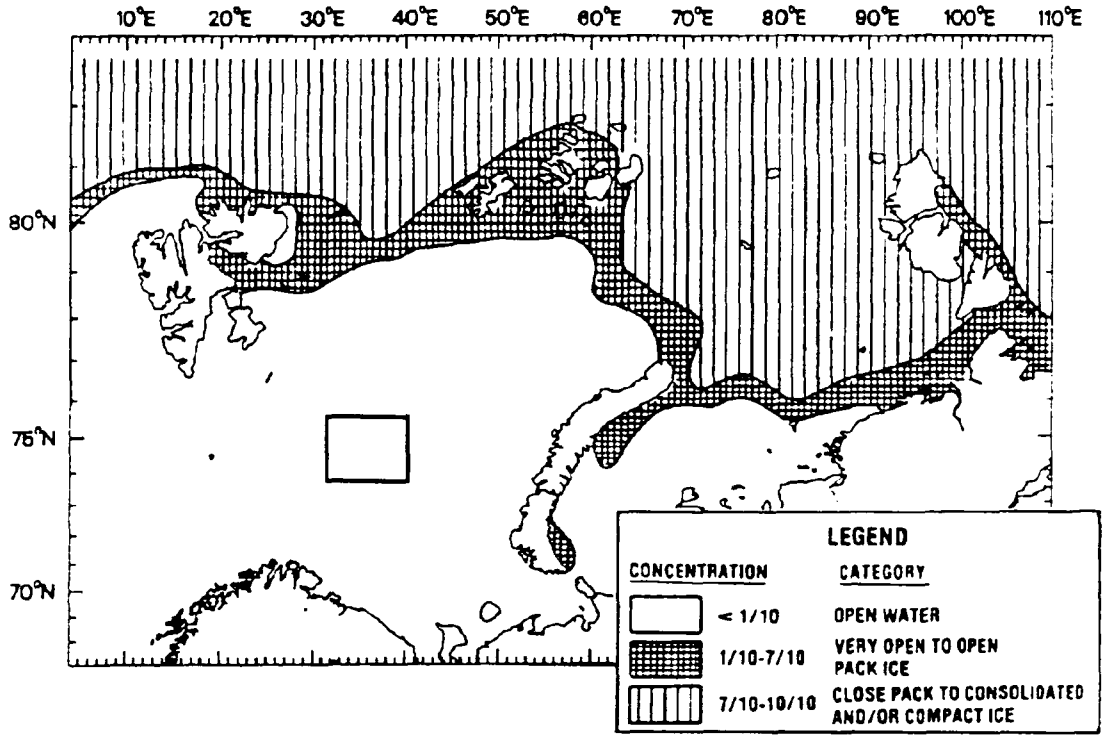

Figure 2.2 Maximum extent of sea ice in the Barents Sea in August (NAVOCEANO, 1990). The box indicates the location of the study area.

B. CIRCULATION

The current pattern in the Barents Sea has been the subject of intense scrutiny since the turn of the century. Helland-Hansen and Nansen (1909) made the first accurate charts; many other charts have since been developed. Novitskiy (1961) explored the permanent currents of the northern Barents Sea while Loeng (1991) has made the most detailed study of the oceanography of the region; his depiction of the surface current pattern is shown in Figure 2.3.

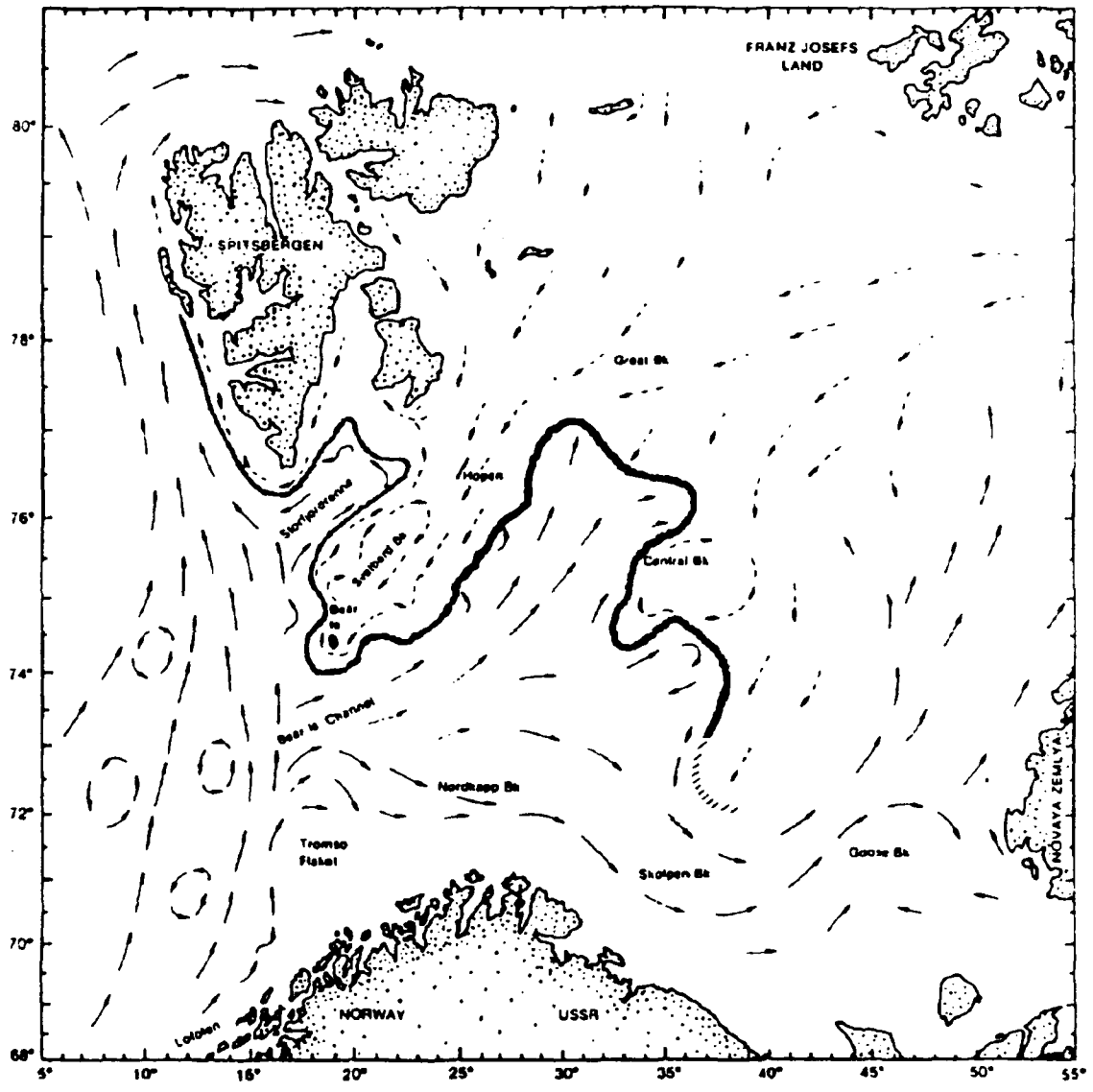

Figure 2.3 Surface currents in the Barents Sea. Solid arrows indicate warm currents, dashed arrows indicate cold currents (Loeng, 1991).

The general circulation of the Barents Sea is forced by a number of factors; prevailing winds, bathymetry, and perturbations of the tangential pressure of the prevailing wind field (Novitskiy, 1961). The form of the general circulation pattern is not influenced by the volume transport

into and out of the Barents Sea, i.e., the flow pattern is independent of water exchange (Loeng, 1991). The most important factor controlling the circulation appears to be the prevailing winds which set the upper and intermediate waters of the Barents Sea in motion. The only water mass which is immune to wind forcing is Barents Sea Bottom Water (BSBW) which follows a flow pattern driven by topography and brine drainage (Loeng, 1991).

A careful examination of Figure 2.3 reveals that the surface currents form a general cyclonic motion, accompanied by smaller anticyclonic and cyclonic gyres throughout the sea. The pattern is maintained by the factors mentioned above, with the large scale pattern controlled more by the prevailing winds, and the smaller scale patterns by the bathymetry and the perturbations of the tangential wind field. Note the strong inflow of Atlantic Water in the southwest, and the opposing inflow of Polar Water from the northeast. Figure 2.3 shows the charted directions of the surface currents. These are also the directions of the subsurface flows, with a few notable exceptions discussed later.

The Norwegian Coastal Current (NCC) enters the Barents Sea along the Norwegian coast as a shallow current in summertime. It carries relatively high salinity, warm water into the Barents Sea, but is confined to a narrow band which hugs the coasts of Norway, Finland, and the Russian Republic until it reaches the White Sea. In wintertime the NCC is not

observable due to mixing caused by winter storms in the Norwegian Sea making its temperature-salinity (T-S) properties similar to that of the Norwegian Atlantic Current.

The Norwegian Atlantic Current flows into the Barents Sea along the Bear Island Trough (or channel), and changes its name to the Nordkapp Current (Norina, 1968). The Nordkapp Current splits into a southern branch, the Murman Current, and a northern branch the Høpen-Bjørnøya Current. The Murman Current itself breaks into several branches, but the main flow carries Atlantic Water far into the Barents Sea.

Water of Arctic origin enters mainly north of Novaya Zemlya, but a small contribution from the Kara Sea around the southern end of Novaya Zemlya also occurs (Figure 2.3). Yet another contribution of Arctic Water comes in via the East Spitsbergen Current, which flows generally southward, between Svalbard and Franz Joseph Land (Figure 2.3).

C. WATER MASSES

The current system carries with it water of both Arctic and Atlantic origin. These two water masses have vastly dissimilar T-S characteristics (Table 2.1) which makes for relative ease in tracing the water masses as they coarse through the expanse of the Barents Sea. As with the current systems, many researchers have made charts and tables of the water mass structure of the Barents Sea. Norina (1968) identified three major water masses and nine subgroupings

Table 2.1 Barents Sea Water Masses (after Loeng, 1991)

MAJOR TYPES	T (°C)	S (psu)
Atlantic (NAW)	> 3.0	> 35.0
Arctic (AW)	< 0.0	34.3 - 34.8
Coastal (CW)	> 2.0	< 34.7
LOCAL VARIANTS		
Meltwater (MW)	> 0.0	< 34.2
Svalbard Bank (SBW)	1.0 - 3.0	< 34.4
Bottom Water (BW)	< -1.5	> 35.0
Barents Sea Water (BSW)	-1.5 - 2.0	34.7 - 35.0
Polar Front Water (PW)	-0.5 - 2.0	34.8 - 35.0

based on physical properties. A more recent investigation presented by Loeng (1991) includes a system of three major water masses and five locally formed variants (Table 2.1). Figure 2.4 shows Loeng's representation of the geographic regions occupied by each water mass, except the seasonal melt water (MW).

The formation of bottom water in polar regions has been studied at length by Midttun (1985), Swift et al. (1985), and Sarynina (1969) among others. Two general types of bottom water have been found to form in the Barents Sea. The first is formed through the process of brine rejection during sea ice formation and is a more or less a regular wintertime

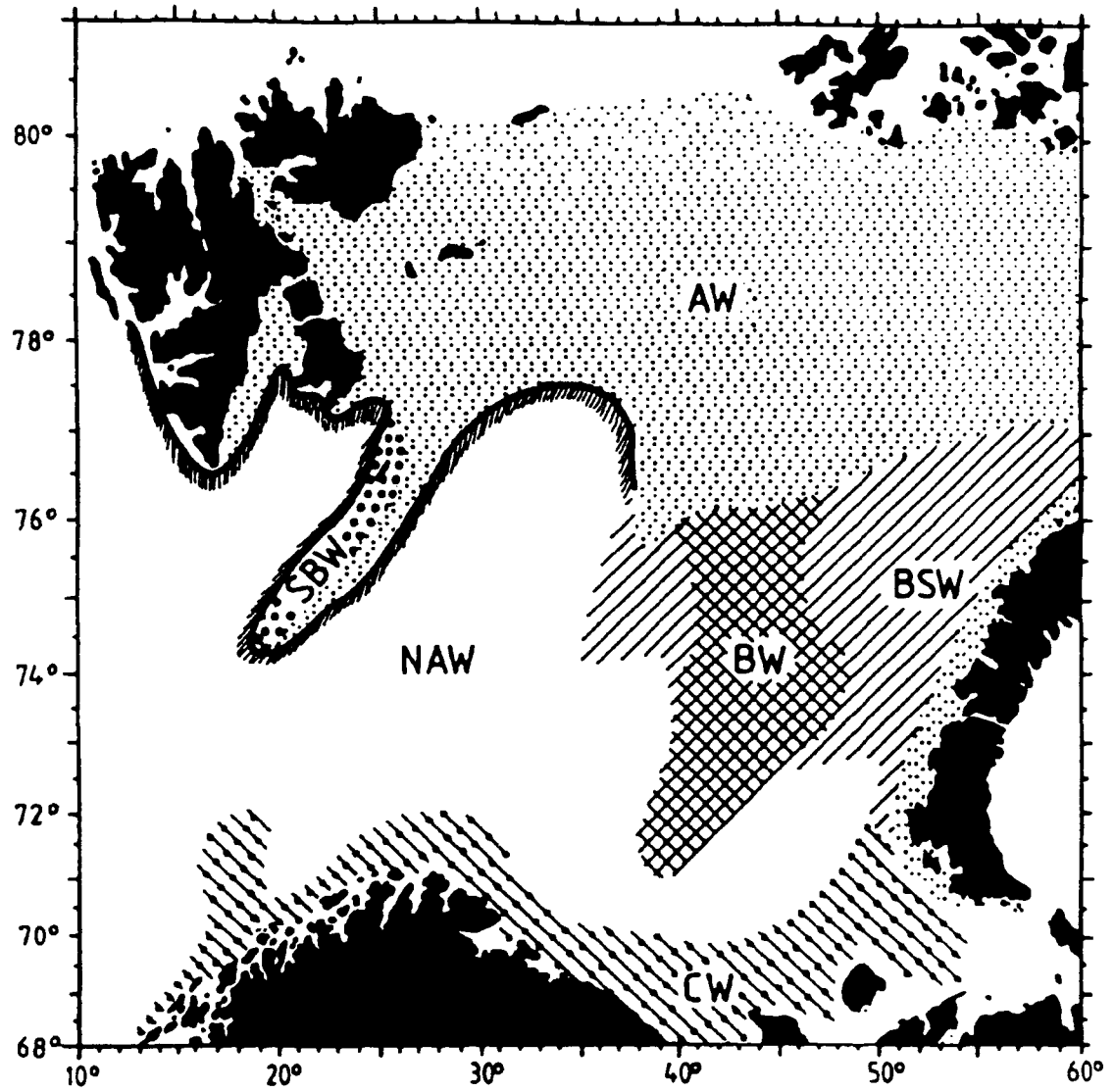

Figure 2.4 Geographical distribution of water masses in the Barents Sea (Loeng, 1991). The Barents Sea Polar Front is defined by the shaded line. Water masses are described in the text.

phenomenon, particularly on the shelf west of Novaya Zemlya, and may also occur on the south eastern Spitsbergen Bank (Figures 2.1 and 2.4) (Midttun, 1985). Midttun (1985) also postulates the existence of a lower salinity bottom water formed over the Central Bank in the winter season. This water

is carried downward by convective mixing which occurs during the winter and mixes with the bottom water formed on the western Novaya Zemlya shelf.

The bottom water formed on the Central Bank and the western Novaya Zemlya shelf flows into the depression of the Central Basin (Figure 2.1) and may fill it completely before being purged by inflowing North Atlantic Water (Loeng, 1991). This Central Basin Bottom Water flows out of the Barents Sea through the Polar Trough, north of Novaya Zemlya, and contributes to the total bottom water of the Arctic Ocean.

During the winter months convective overturning occurs throughout the Barents Sea. Convection may reach to the bottom in shallow areas like the Central Bank and contribute to bottom water formation. In deeper water regions where convective overturning does not extend to the bottom it may extend to 200 m making temperature and salinity homogenous to this depth (Midttun and Loeng, 1987).

The bottom water formed on the Svalbard shelf is carried southward into the Bear Island Trough during the period of winter convective overturning over the southeastern slope of the Spitsbergen Bank (Sarynina, 1969). This Bear Island Trough Bottom Water may be warmer than +1°C and only reaches the bottom of the trough due to convective overturning (Midttun and Loeng, 1987).

As shown in Table 2.1, NAW introduces warm saline water into the Barents Sea while AW introduces cold, relatively

fresh water into the system. The juxtaposition of these flows creates the Barents Sea Polar Front, the subject of the next section. As in many frontal situations in the ocean, the front does not extend to the bottom. In the Barents Sea the meeting of the saltier, denser NAW and the fresher, lighter AW forces the NAW to subduct under the AW. The NAW flows at depth to approximately 40°E (Dickson *et al.*, 1970). The result is that the Barents Sea Polar Front is confined to the upper one third of the water column.

The locally variant water masses PW, CW, SBW, and BSW have characteristic temperatures and salinities and vertical stratification that separate them from the three major types. CW is a highly vertically stratified water mass particularly during the summer months. This stratification is strongest along the Norwegian coast and weakest in the far eastern portion of the Barents Sea. The stratification is nearly gone in winter due to cooling causing vertical convection resulting in mixing (Loeng, 1991). MW exists only in the summer months and overlays the AW north of the Polar Front to a depth of 5-20 m (Loeng, 1991). MW is formed as a result of the summertime melting of sea ice and in cold years, with very heavy ice formation, MW may form a thin layer south of the Barents Sea Polar Front as drifting ice sheets and bergs melt (Loeng, 1991).

AW in the eastern Barents Sea is transformed by the processes of ice formation and melting (Midttun, 1985) and

mixes with the resident AW to form BSW (Loeng, 1991). BSW is found overlaying BW in the eastern regions of the Barents Sea (Figure 2.4). PW has characteristics similar to BSW (Table 2.1) but is found in the western Barents Sea along the Polar Front (Loeng, 1991).

The last local variant, SBW, is a summertime mixture of AW and atmospherically warmed MW. These two water masses mix in the large gyre on the central portion of the Svalbard Bank (Figure 2.3). The SBW exists only during the summer season and is completely replaced during the colder seasons by AW. (Loeng, 1991).

D. BARENTS SEA POLAR FRONT

In the interior of the Barents Sea a weak to moderate oceanic front exists due to the juxtaposition of NAW and AW. The front is delineated by NAW on its southwest margin and AW to the northeast (Figure 2.4). The far western edge of the front, around Bear Island, was studied in detail by Johannessen and Foster (1978). They concluded that in this region the front is topographically controlled along the 100 m isobath (Figure 2.5). The exact extent of the topographic control varies seasonally, but the front follows the 100 m isobath as far east as approximately 76.5°N (Figure 2.4). The front is also topographically controlled along the steep slope of the western edge of the Central Bank (Loeng, 1991a).

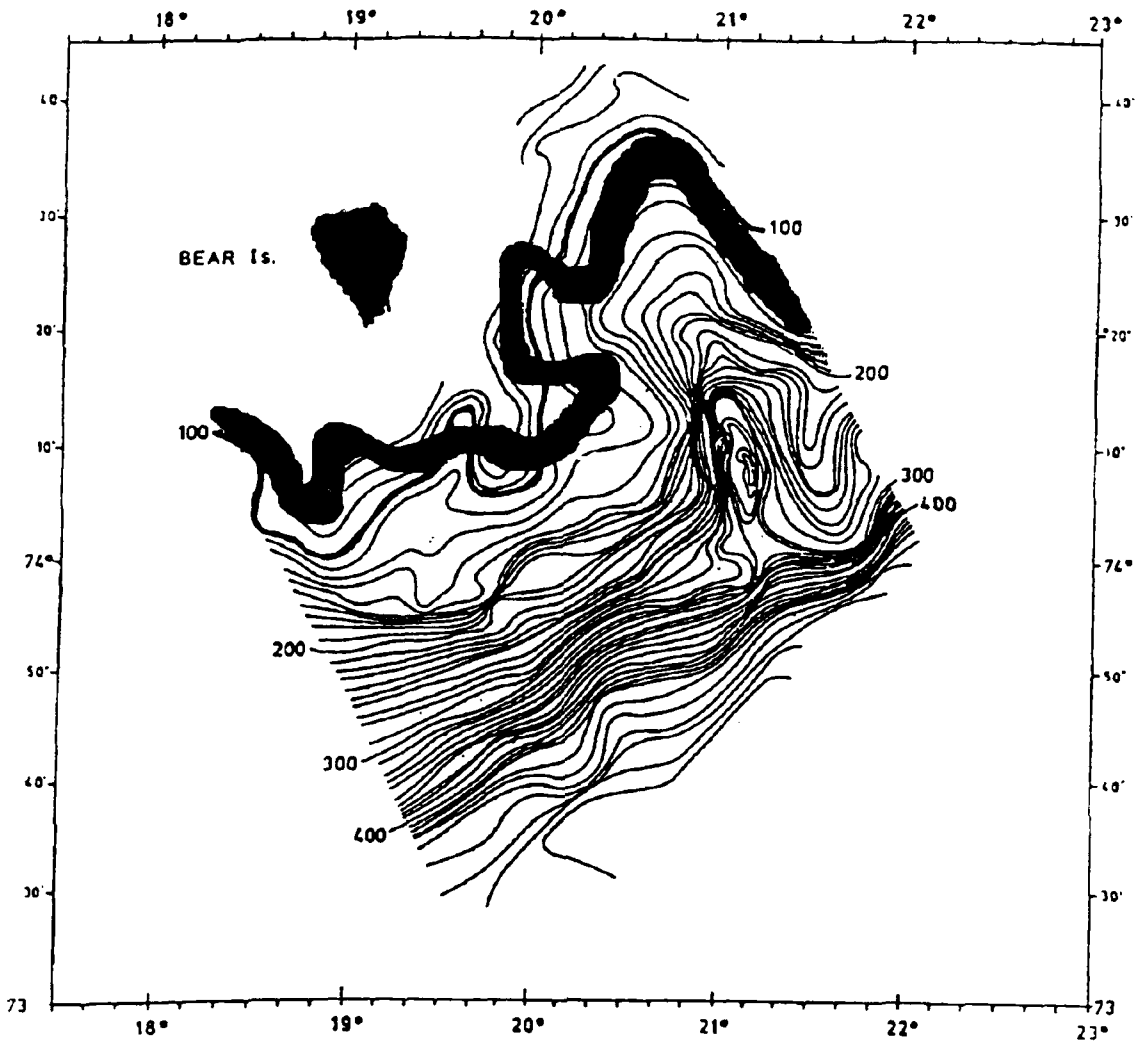

Figure 2.5 Bathymetricaly controlled section of the Barents Sea Polar Front (broad line) around Bear Island (Johannessen and Foster, 1978)

The frontal position is controlled by the inflow of NAW in most of the other regions of the Barents Sea. The front veers away from the 100 m isobath at approximately 77.5°N and meanders under the influence of currents until it is again topographically controlled along the western slope of the Central Bank. In the region east and south of the Central Bank the front is less distinct with large areas of the

eastern Barents Sea being covered by BSW. In this region the classical definition of a front can not always be applied (Loeng, 1991a).

The position of the front as discussed above is a seasonal mean position (Figure 2.3). The frontal core oscillates with the tides and with the seasons. The tidal oscillation has been well studied and is on the order of 10 km/cycle around Bear Island (Johannessen and Foster, 1978). However, the mean seasonal and yearly positions vary as a function of location and climate (i.e., the boundary is particularly sensitive to North Atlantic storms). In the region near Bear Island, where topography guides the front, the seasonal variation is about 50 km/year (NAVOCEANO, 1991). It is less easy to define precise limits for regions where the front is not so closely linked to the topography. In-depth studies of the front in regions well removed from Bear Island have not been conducted (Loeng, 1991a).

The Barents Sea Polar Front plays a pivotal role in determining the extent of sea ice each winter. Ice forms rapidly throughout the northern Barents Sea in late September and advances rapidly southward reaching the summertime position of the Polar Front in November or December (Midttun and Loeng, 1987). The position of the maximum ice edge changes from year to year in response to environmental changes in the Barents Sea which are driven predominately by the inflow of

NAW (Loeng, 1991). The forces driving the inflow of NAW will be discussed in the section on Climatology to follow.

The Barents Sea Polar Front is characterized by a change in temperature of 5°C and a change in salinity of 1 psu over the 100 km of its horizontal extent around Bear Island (Dickson *et al.*, 1970). In the region of the Central Bank the front is weaker with a 5°C temperature change and 0.5 psu salinity change over 150 km (Dickson *et al.*, 1970).

The acoustic influence of the Barents Sea Polar Front can be significant depending upon the strength of the horizontal temperature gradient across the front and thus this influence varies over the extent of the front. Heathershaw *et al.* (1989) established that the strong oceanic front of the Gulf Stream can introduce propagation loss increases on the order of 20 dB, and can introduce horizontal refraction effects of greater than 1°. The effect of the Barents Sea Polar Front should be less due to its narrow horizontal extent, and weak ΔT and ΔS compared to the Gulf Stream, but still significant based upon the results of this study (Chapter IV). A detailed knowledge of the location of the front and the corresponding temperature and salinity gradients are essential in the modeling of propagation of sound.

E. GEOLOGIC STRUCTURE

1. EVOLUTION OF THE SEA FLOOR

The Barents Sea covers the northwestern most portion of the Eurasian shelf and is known to geologists as the "Barents Shelf" (Eldholm and Ewing, 1971). The present boundaries of the Barents Sea were established near the end of the Tertiary period and the final contours delineated in the Quaternary period (Klenova,1961). The features of the Barents Sea floor and surrounding land areas have evolved over a long and complex geologic history which was influenced by several factors.

Svalbard and Norway drifted apart about 38 million years ago (mya) forming a low, flat region now known as the Barents Sea. This region underwent a number of uplifts and subsidences with corresponding regressions and transgressions of the sea over the region (Freebold, 1951). The last principal regression occurred during the middle Cretaceous, and the main part of the Barents Shelf was not covered again by the sea until the Quaternary (0.7 mya) (Eldholm and Ewing, 1971).

Another factor influencing the development of the Barents Shelf was glaciation. As with all Arctic regions the Barents Shelf has been repeatedly covered and uncovered by glacial ice sheets. Active glaciers still exist on Novaya Zemlya, Franz Josef Land, and Svalbard (CIA, 1978). The last and most

extensive glacial event occurred during the Pleistocene epoch, 1.5 mya, and receded at about the same time as the Quaternary subsidence 0.7 mya (Eldholm and Ewing, 1971). The southernmost portion of the Barents Sea remained ice free, most likely due to the warm water influence of the Norwegian Coastal Current (Sach and Stelkov, 1961). The passage of these glaciers carved out deep valleys and deposited large amounts of sediment on the slopes of rises, and left submarine moraines at the northern margin of the sea (Batrurin and Yunov, 1990).

F. CLIMATOLOGY

The Barents Sea is situated in a geographic position that permits more temperate conditions than are found in other Arctic regions of similar latitude (Welsh et al., 1986). The inflow of NAW carrying remnants of the warm Gulf Stream and the presence of prevailing winds from the south leads to these temperate conditions. However, the high latitude location (70°-80°N) makes the region subject to the extended days and nights typical of the polar region (Figure 2.6). These effects combine to produce an Arctic sea which is partially ice free year round, and contains one of the most complex and unstable water mass structures found anywhere in the world (Welsh et al., 1986).

Detailed study of the climatology of the Barents Sea region begin at the beginning of this century with the

Russians conducting monthly meteorological observations off the Kola Peninsula from 1900-1906, and 1920-present (the period 1941-1944 was not measured due to the Second World War, and the period 1906-1920 was measured only quarterly) (Midttun and Loeng, 1987). Nansen (1906) and Helland-Hansen and Nansen (1909) made oceanographic surveys of the region and advanced theories on bottom water formation. They postulated an advective nature to the observed climatic variations and measured a 1 year time lag between oceanographic events at the eastern edge of the Barents Sea and corresponding events on its western side (Loeng, 1991). More recent and detailed studies have verified the advective nature of the climatic variations and demonstrated a time lag of approximately 6 months (Loeng et al., 1983).

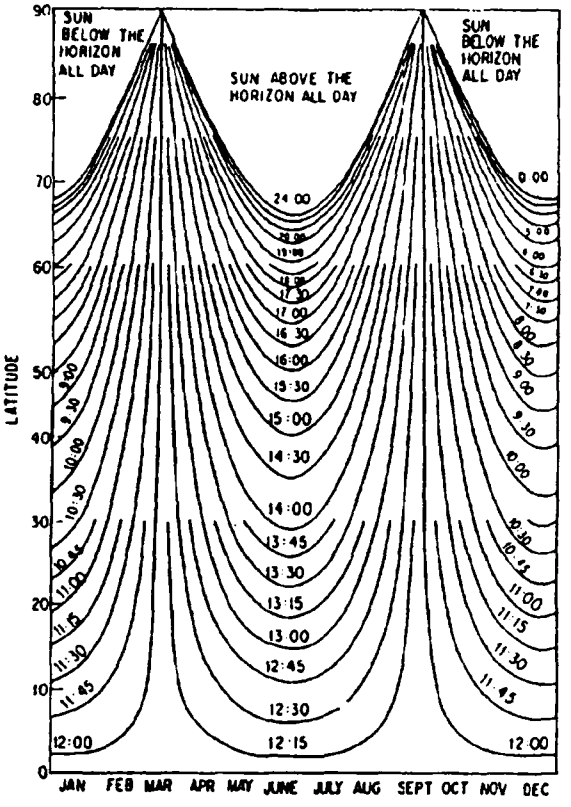

Figure 2.6 Latitudes and dates for duration of daylight (Gathman,1986)

The climate of the Barents Sea is strongly linked to the inflow of NAW. The transport rate of NAW into the Barents Sea is itself governed by the wind stress (Loeng, 1991). This flow of warm, high salinity water into the Barents Sea drives

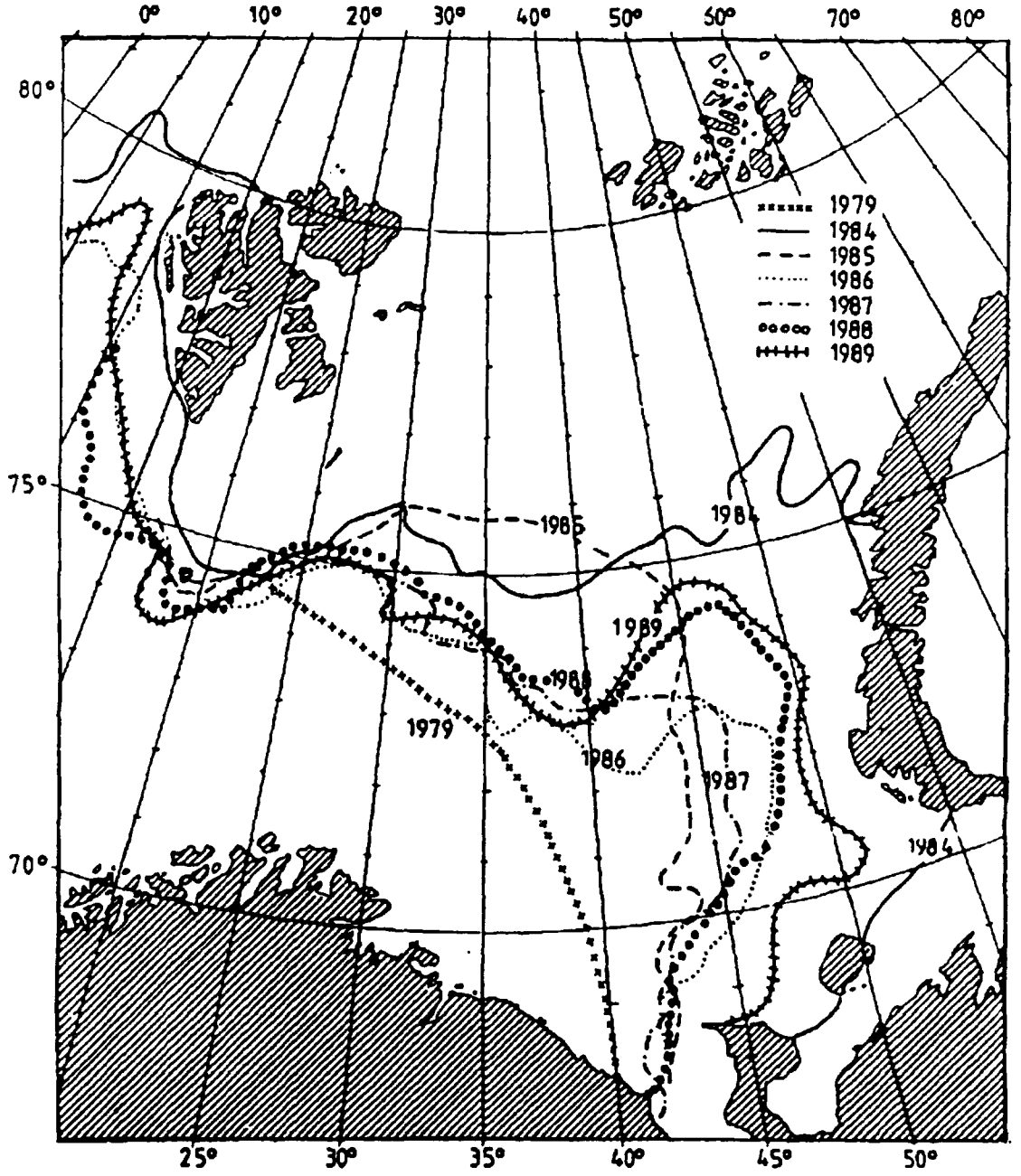

Figure 2.7 Sea ice maxima for several years in the 1980's (Loeng, 1991).

nearly all of the processes occurring there. The strength of the Polar Front is directly dependent upon the T-S properties of the NAW and AW, while the purging of BW out of the Central

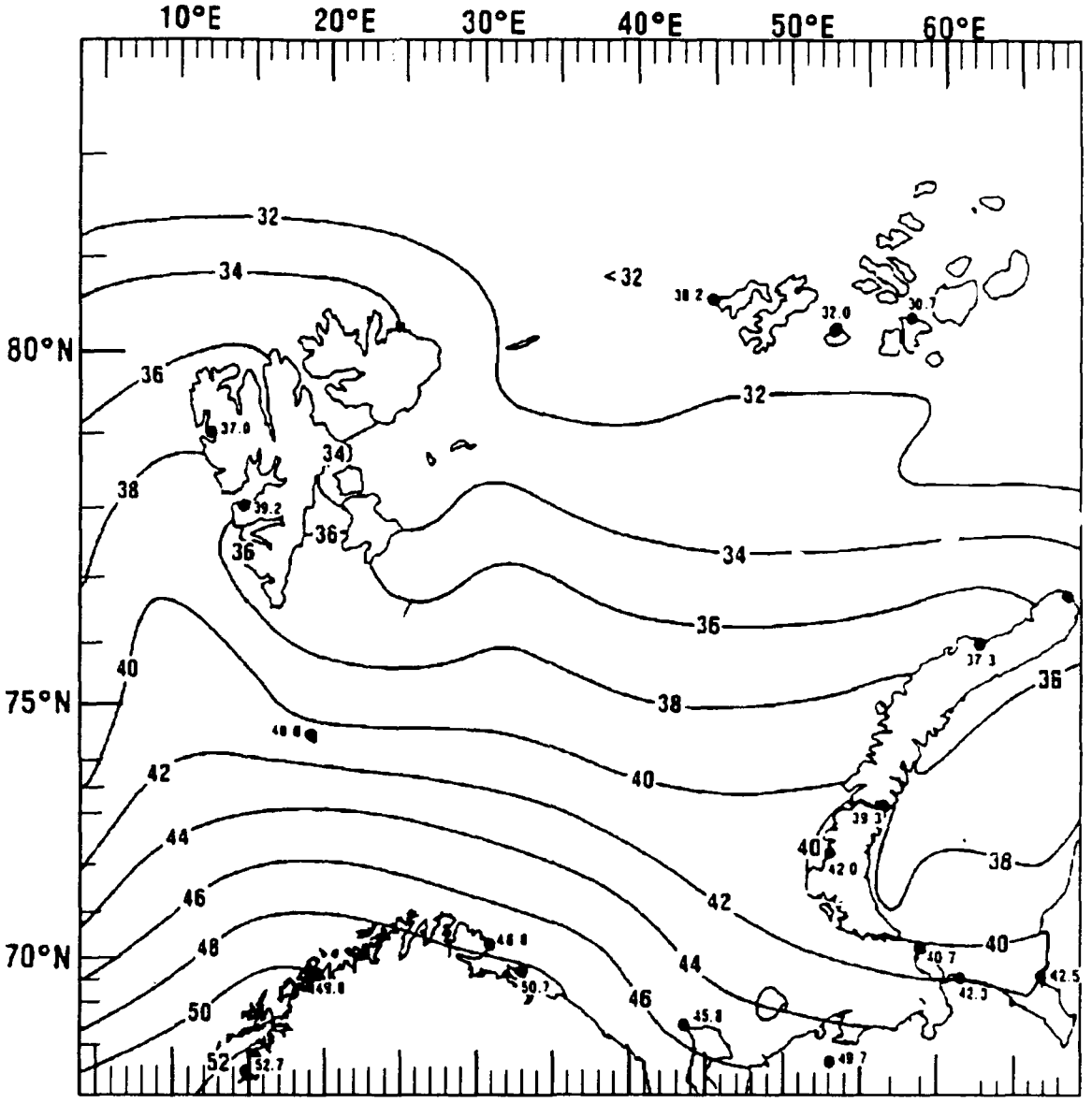

Figure 2.8 Mean air temperature in the Barents Sea in August (°F) (NAVOCEANO, 1991).

Basin depends upon the transport rate of NAW into the Sea (Midttun, 1985). Large influxes of NAW can result in minimum sea ice extent the following year, a feature which occurred twice in the 1980's. The first was the winter of 1982-83, and again in 1989-1990 when a maximum of NAW transport into the

Barents Sea resulted in a nearly complete purging of Bottom Water from the Central Basin. The resulting replacement of cold Bottom water with warm NAW resulted in an extreme sea ice minimum in 1984 (Figure 2.7) (Loeng, 1991).

The air temperature in the Barents Sea (Figure 2.8) also shows the North Atlantic influence. Air temperatures are influenced by extratropical storm systems which regularly pass through the Barents Sea (Gathman, 1986). The mean summer air temperature in the Barents Sea is 8°C (CIA, 1978). Figure 2.9 shows the composite storm tracks for all seasons from the years 1944-1951. The winter months are characterized by strong cyclonic circulations, influenced by the semi-permanent low pressure cell near Iceland. The passage of these systems through the region leads to a moist adiabatic lapse rate in the atmosphere above the Barents Sea. The summer months are influenced by the increase in solar input, due to the longer days, and a decrease in cyclonic activity from the North Atlantic. The melting of sea ice leads to Polar maritime air shifting considerably farther north during summer than winter (Gathman, 1986). The stability of the atmosphere increases in summertime as the cyclonic activity deceases (Gathman, 1986).

Another effect of the warm air and water systems moving through the Barents Sea is abundant precipitation and cloud cover. The frequency of precipitation in the period July-September (Figure 2.10) in the Central Bank region is greater than 20%. Extrapolating the inches of rain fall shown on

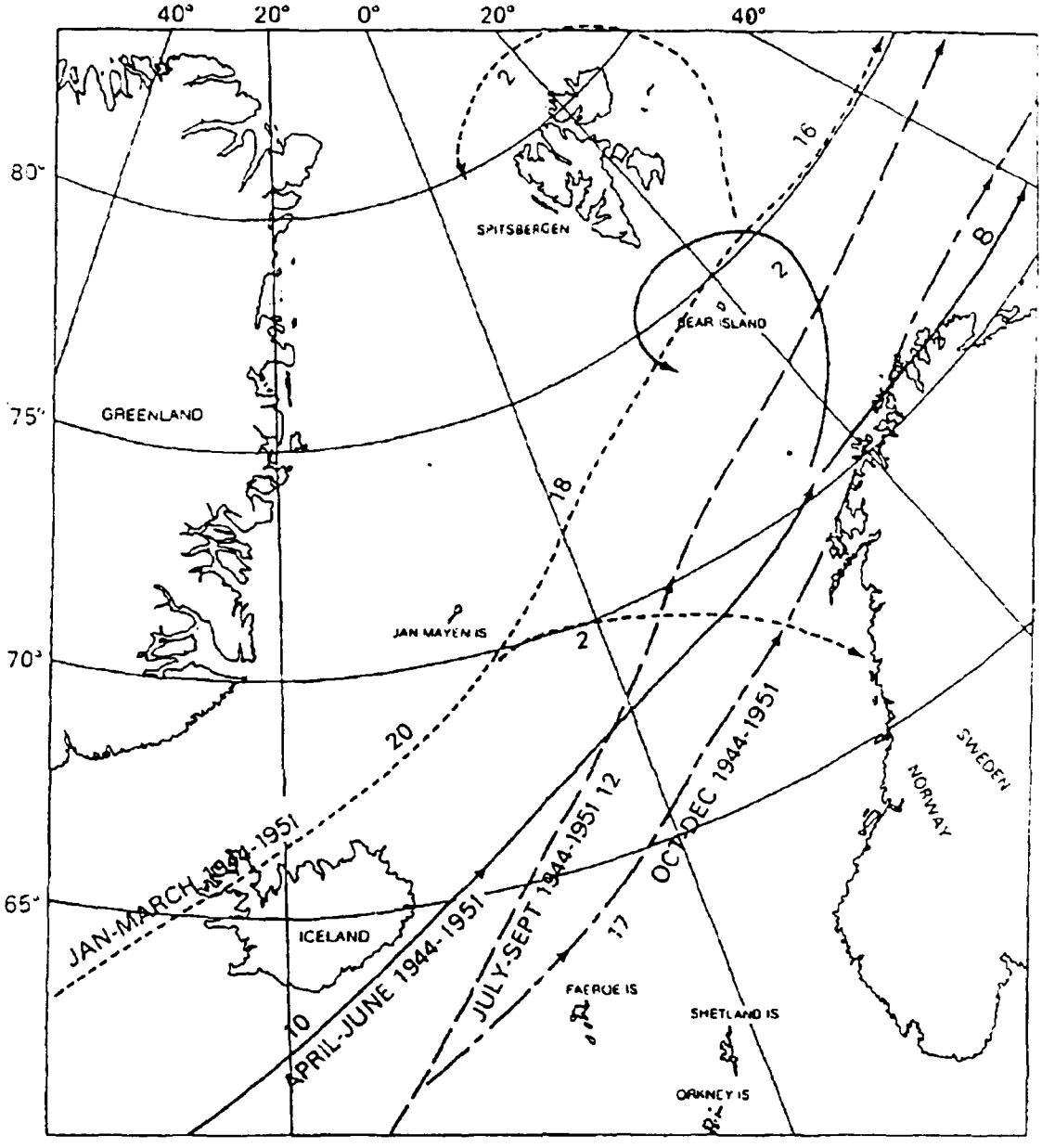

Figure 2.9 Mean tracks of severe low-pressure centers. (Numbers along tracks indicate relative frequency of storms) (Gathman, 1986).

Figure 2.10 from Bear Island (1.27") to Novaya Zemlya (1.95") the expected rain fall in the area of the Central Bank is around 1.7" from July to September. The percentage of 5/8 or greater coverage of low clouds over the central Barents Sea

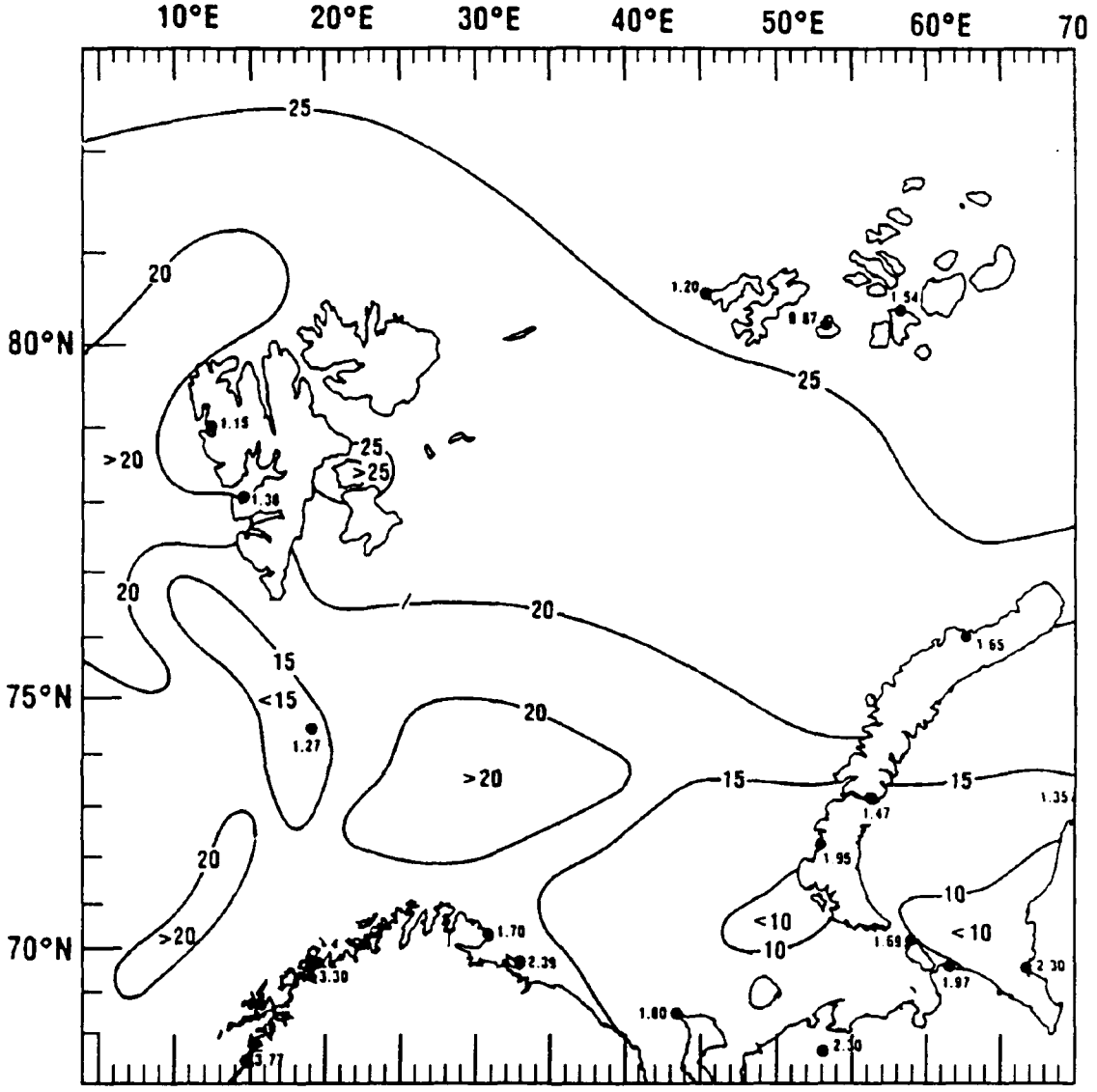

Figure 2.10 Percent frequency and amount (in.) of rain in the Barents Sea during the period July to September (NAVOCEANO, 1990).

during summer (Figure 2.11) is 85%. The frequency of low ceilings (< 600 ft), and/or < 2 nmi visibility is 15-30 % (NAVOCEANO, 1990). Thus during the Barents Sea Acoustic Tomography Transmission Test one can expect overcast skies,

periods of sharply reduced visibility, and abundant precipitation (NAVOCEANO, 1990).

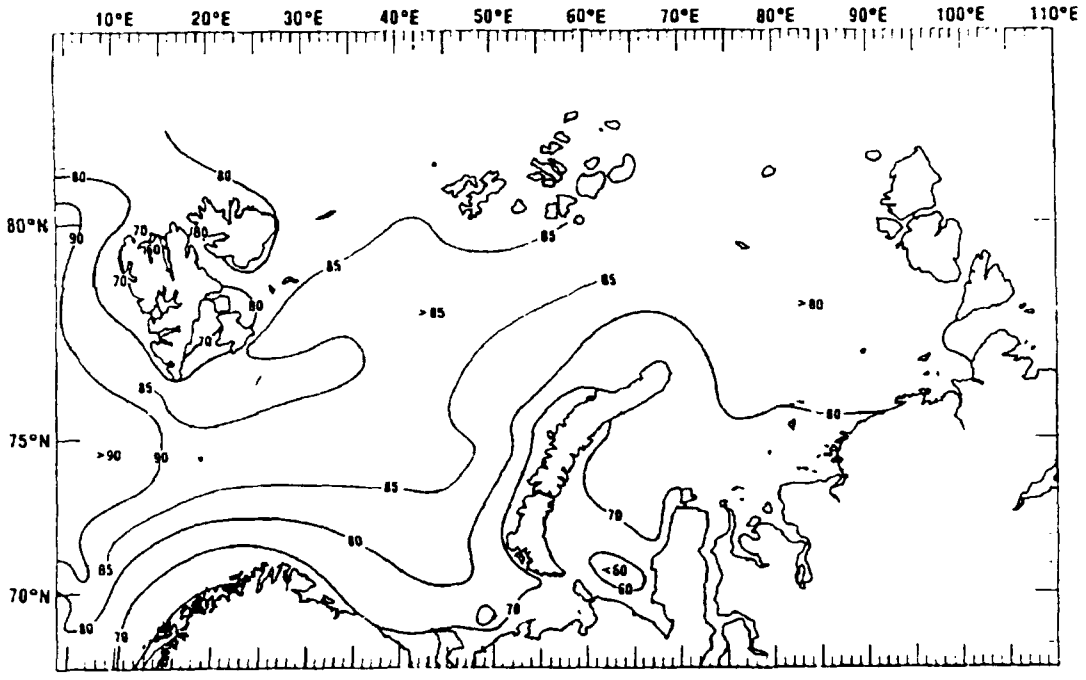

Figure 2.11 Percent frequency of 5/8 or greater coverage by low clouds (< 8000 ft) (NAVOCEANO, 1990).

Another issue of interest in the execution of any operation at sea is the expected sea state and accompanying wave heights. The open ocean areas of the Barents Sea have seas in excess of 1.5 m 20-50% of the time (Welsh et al.,1986). Figures 2.12 and 2.13 show the mean wave height in feet, and the percent frequency of wave heights of 12 ft or greater in the summer months of July - September, respectively (NAVOCEANO, 1990). Note that the Central Bank region has mean summer wave heights of 3 feet or more, with seas greater than 12 feet approximately 5% of the time. There is a greater than

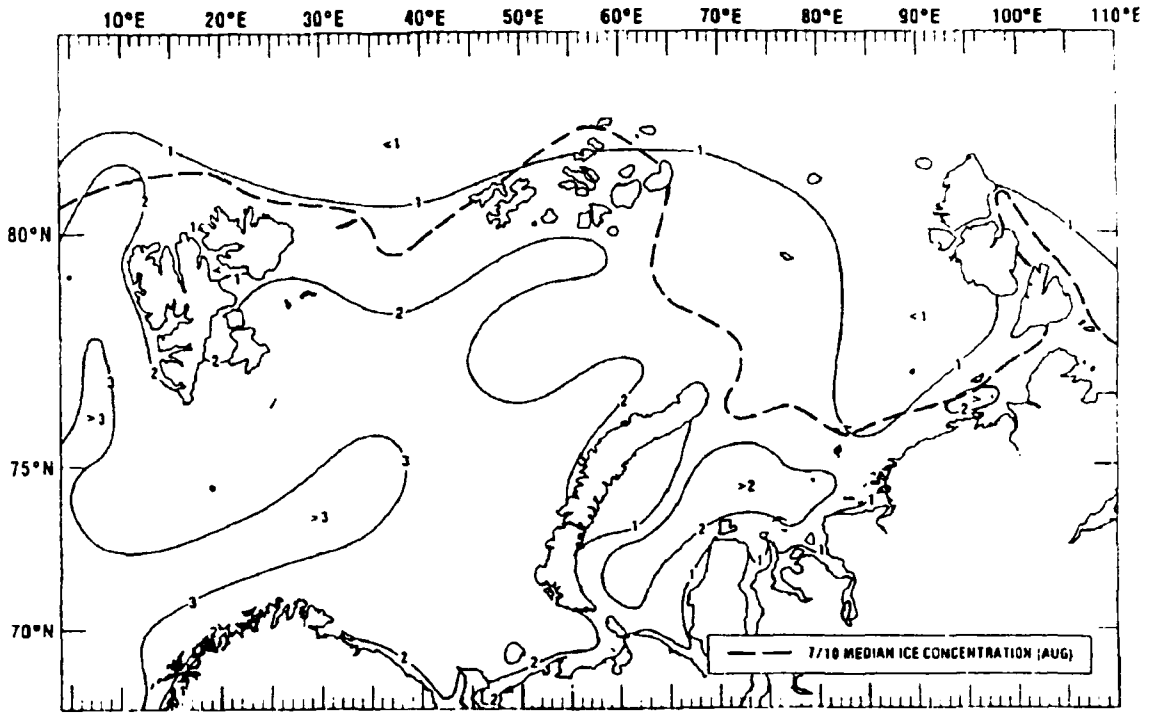

Figure 2.12 Mean wave height (ft) for the period July to Sept. (NAVOCEANO, 1990).

1% chance of seas greater than 20 ft (Figure 2.13); these high seas are related to the passage of severe North Atlantic storms through the Barents Sea. The schedule of the test can be affected by storm passage through the Barents Sea. The roughness of the sea surface can greatly effect the propagation of sound in the ocean; the effects of sea surface roughness on the propagation of sound will be discussed in Chapter III.

In summary the environmental conditions during the months of August and September should be acceptable for the conduct of an ocean acoustic tomography experiment. The sea ice edge

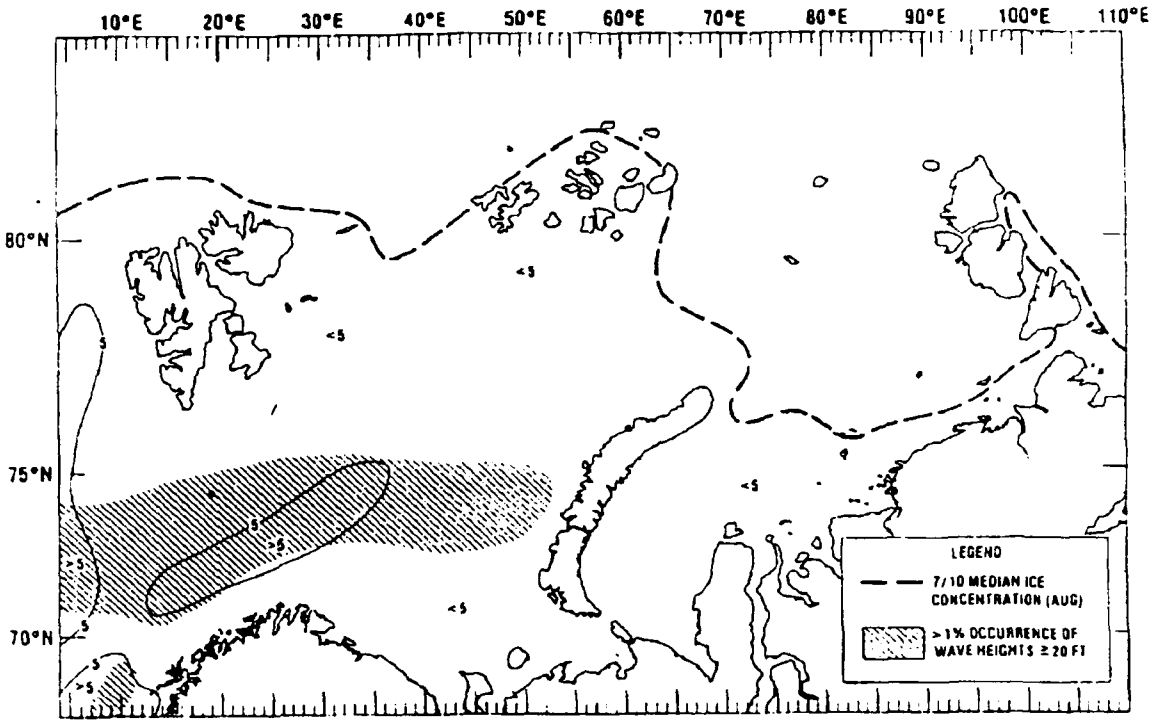

Figure 2.13 Percent frequency of wave heights 12 ft or greater in the period July to Sept. (NAVOCEANO, 1990).

should be well north of 77° N, the wave height should average about 1 m with the air temperature a temperate 6-15°C. These conditions, though far from ideal, should provide an acceptable environment for the positioning of the bottom moored sources and receivers, and for the safe navigation of the Barents Sea by the vessels involved.

III. Acoustic Effects

A. Introduction

The study of the propagation of sound in the ocean requires an understanding of the properties of the ocean medium and its boundaries, and their influence upon sound propagation. There are many factors to consider in the ocean environment. Urick (1983), Kinsler *et al.* (1982), and Clay and Medwin (1977) among others present detailed descriptions of these factors which include: ambient noise, absorption, spreading, surface and bottom interactions being the principle factors.

This chapter will examine those factors which can reasonably be expected to influence the propagation of low frequency sound for this experiment. The culmination of this discussion will be an examination of the sonar equation as it applies to the Barents Sea Acoustic Tomography Transmission Test.

B. Bottom Interactions

Below the water-sediment interface are often many layers of deposited sediments above the basaltic layers of bedrock of the subfloor (Clay and Medwin, 1977). As discussed above, a

large number of *in situ* sound velocity[3] measurements have been made for the Barents Sea floor as well as many laboratory measurements available from core samples (Orsi and Dunn, 1991). *In situ* measurements, although more difficult to obtain, are generally more accurate than laboratory measurements because the coring procedure disturbs the sediment structure (Clay and Medwin, 1977).

Until the late 1960's little was known about the bottom structure of the Barents Sea. In 1968-1969 R/V Vema made several traverses of the southwestern Barents Sea making a wide variety of oceanographic and acoustic measurements (Eldholm and Ewing, 1971). Since then many other expeditions and experiments have been conducted producing a large set of sonobuoy, CTD, XBT, magnetic, gravity, and bathymetric data (Eldholm and Talwani, 1977).

The episodic nature of the uplifting and subsidence of the Barents Shelf has left a complex pattern of layered sediments on top of the mesozoic bedrock (Klenova, 1966). Figure 3.1 shows the detailed patterns of the sediments found in the Barents Sea. The deposition of sediment during all periods of history has been a function of river run off, topography, current structure, and subsidence rate (Eldholm and Talwani, 1977). Present day river run off into the Barents Sea is

---

[3]. The term velocity is used here rather than speed because the direction of propagation is important in solids, where as this is not true of fluids (Clay & Medwin, 1977).

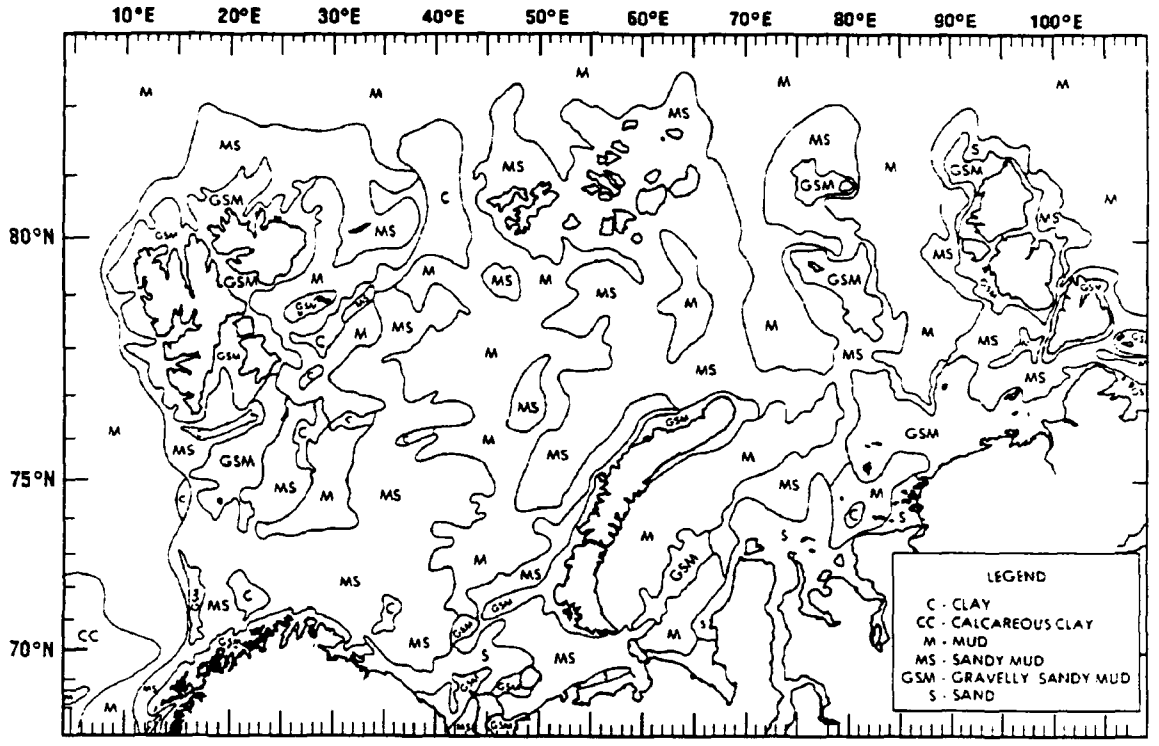

Figure 3.1 Sediment distribution in the Barents Sea (NAVOCEANO, 1990).

practically non-existent, with the exception of the Petchora River (Klenova,1966). The mechanical filtering of sediment by the large scale tectonic features is evident as larger grained materials collect around the submarine rises where the currents cannot carry them up the steep slopes. The slopes of the rises are covered with varying thicknesses of local sediments and glacial deposits. The tops of the rises are covered with poorly sorted smaller grained materials which rarely settle long enough to collect to an appreciable depth (Klenova, 1966).

The propagation of sound in a fluid is of a purely compressional nature, i.e., there is no shear wave propagation

(Kinsler *et al.*, 1982). Shear waves, however, can be excited in the sediments due to the structural rigidity of the solid materials, and thus one must consider both compressional (c_{p2}) and shear wave (c_{s2}) speeds in sediments. Both components of the sound velocity in the sediments are required to accurately calculate the water-sediment interface reflection coefficient ($\Re_{12}$).

The acoustic properties of these sediments have been measured using sonobuoys and air guns in several studies (Houtz and Windisch, 1977; Houtz, 1980). Houtz and Windisch (1977) used a modified T^2/X^2 technique[4] (LePichon et al., 1968) that computes the average sound velocity in the layer between two adjacent reflecting interfaces. The limitation of this technique is that it does not resolve a layer thinner than 300 m and for this reason the uppermost sediments remain undetected (Houtz, 1980). To overcome this deficiency Houtz (1980) presented a method to measure the near-seafloor sound velocities using a multiple reflection technique. Katz and Ewing (1956) developed the method adapted by Sutton and Maynard (1971) and later used by Houtz (1978; 1980) to obtain the sound velocity of the upper sediment layer. Figure 3.2 presents the mean compressional wave velocities in the upper 100 m of sediment. Combining these values with the deeper depth values of Houtz and Windisch (1977) permits construction

[4]LePichon's technique relates travel time to sediment depth.

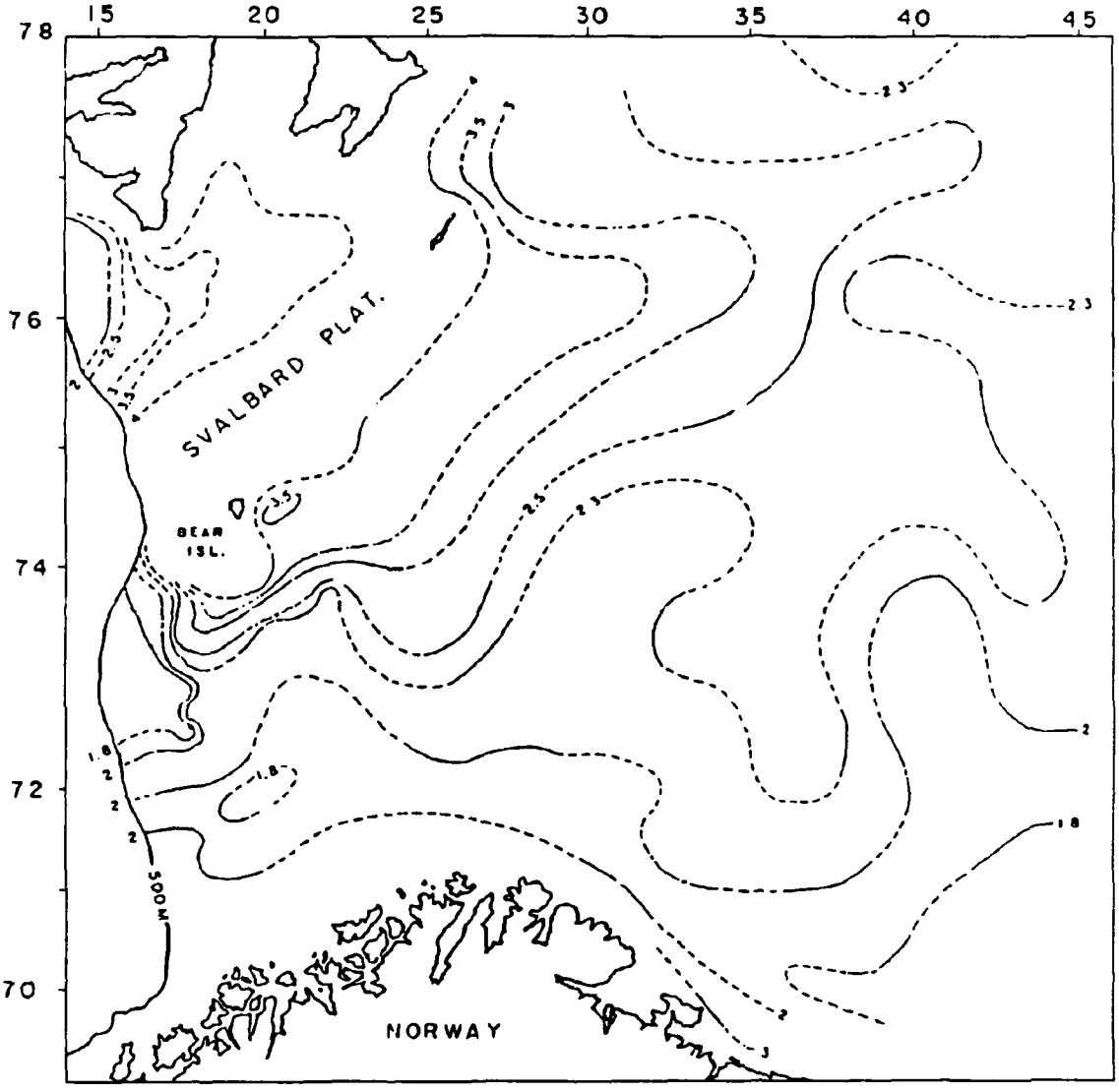

Figure 3.2 Near floor compressional sound speeds. Contours in km/s (Houtz, 1980).

of a composite compressional vertical sound velocity profile for various regions of the Barents Sea. The vertical compressional wave sound velocity profile for the upper 4000 m of sediment over the Central Bank is shown in Figure 3.3. Shear velocities for various sediment types are tabulated in

Clay and Medwin (1977). For a sandy bottom c_{s2} is 503 m/s, or 382 m/s for muddy sand.

1. Calculation of the Bottom Reflection Coefficient

The muddy sand found on and around the Central Bank has shear velocities of approximately 503 m/s (Clay and Medwin,

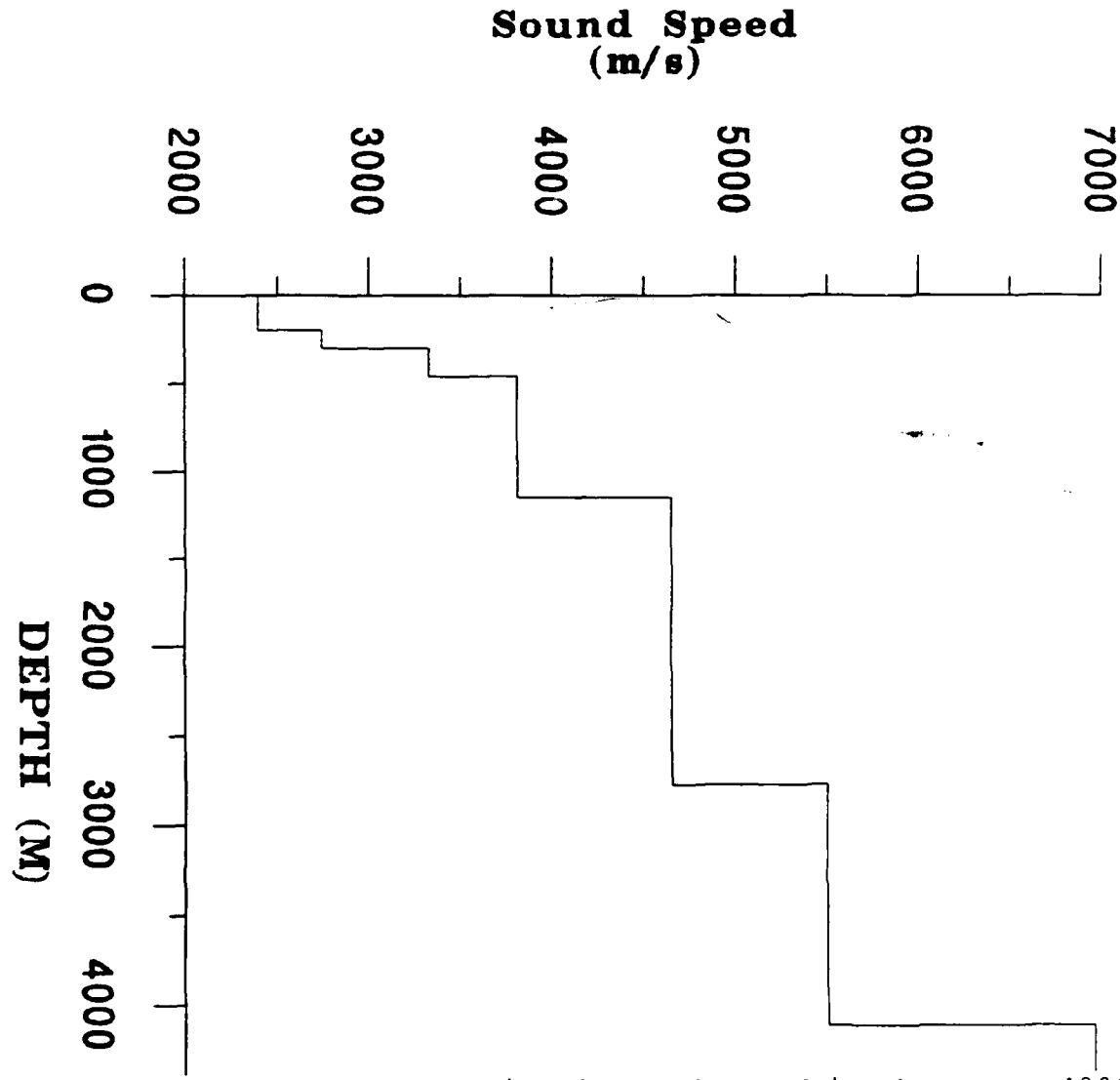

Figure 3.3 Plot of compressional sound speed in the upper 4000 m of sediment.

1991), and compressional speeds of approximately 1640 m/s (Dunn, 1991) in the upper 3 to 5 m of sediment. As the depth of burial of sediments increases, the water is squeezed out of the pores, the porosity decreases, and the shear and compressional velocities increase (Clay and Medwin, 1977). The values of compressional velocity presented in Figure 3.2 are averages for the upper 100 m of sediment and thus are larger than the actual value at the interface.

Reflection coefficient ($\Re_{12}$) at the water-sediment interface can be calculated after the manner of Tolstoy and Clay (1966):

$$\Re_{12} = \frac{4\gamma_2\delta_2\alpha^2+(\delta_2^2-\alpha^2)^2-(\rho_1/\rho_2)(\gamma_2/\gamma_1)(\omega^4/c_{s2}^4)}{4\gamma_2\delta_2\alpha^2+(\delta_2^2-\alpha^2)^2+(\rho_1/\rho_2)(\gamma_2/\gamma_1)(\omega^4/c_{s2}^4)} \quad \text{Eq.3.1}$$

where:

$$\alpha=\frac{\omega}{c_1}\cos\theta \qquad \gamma_1=-\frac{\omega}{c_1}\sin\theta$$

$$\gamma_2=\frac{\omega}{c_{p2}}\left[1-\left(\frac{c_{p2}}{c_1}\cos\theta\right)^2\right]^{1/2} \qquad \delta_2=\frac{\omega}{c_{s2}}\left[1-\left(\frac{c_{s2}}{c_1}\cos\theta\right)^2\right]^{1/2}$$

where c_1 is the speed of sound in water, and c_{p2} and c_{s2} are the compressional and shear wave velocities of the sediments, respectively, and ρ_1 and ρ_2 are the water and sediment densities. Figure 3.4 shows $\Re_{12}$ versus grazing angle (θ) for $0° < \theta < 90°$.

The critical angle is where the plot of $\Re_{12}$ starts to drop off rapidly from 1. The critical angle is approximately 28°. For $\theta \leq \theta_c$, little energy is transmitted into the sediments.

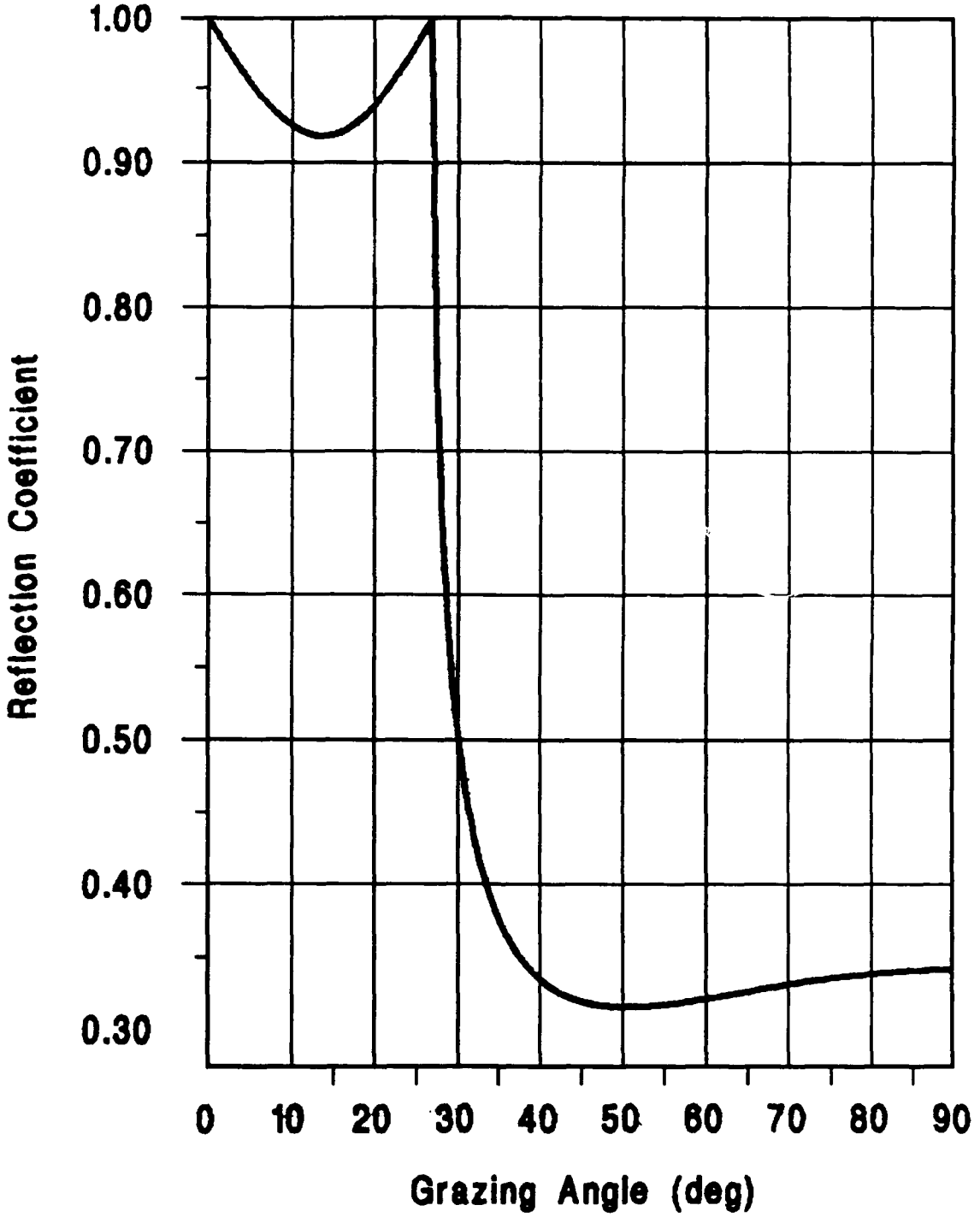

Figure 3.4 Bottom reflection coefficient vs. grazing angle at 224 Hz.

2. Bottom Loss

The energy loss incurred at each interaction of an acoustic ray with the bottom is a function of the bottom type, the acoustic frequency, and the grazing angle (θ). The bottom loss (BL) per bounce is related to $\Re_{12}$ as:

$$BL = -20 \log(|\Re_{12}|) \qquad \text{Eq. 3.2}$$

Figure 3.5 shows BL versus grazing angle for the $|\Re_{12}|$ values displayed in Figure 3.4. Note that for $\theta < 28°$ BL $\approx$ 0 dB/bounce and increases rapidly for $\theta > 28°$ to a maximum value of slightly more than 10 dB/bounce. For the high angle rays, $\theta > 28°$, anticipated in this study approximately 35 bottom bounces can be expected over a 75 km horizontal length of the path, as indicted in our raytracing results. This number of bounces would result in 350 dB of loss due to bottom interactions alone. Thus rays that graze the bottom at angles greater than 28° are attenuated prior to reaching the receiver 75 km down range.

C. SURFACE INTERACTION

1. Calculation of the Surface Reflection Coefficient

In a shallow water sound channel interactions of the acoustic rays with the surface are an important consideration. Each reflection from the surface introduces a reflection loss causing some of the acoustic energy to be incoherently scattered. The most important parameters in the calculation of the reflection loss are surface wave height and acoustic

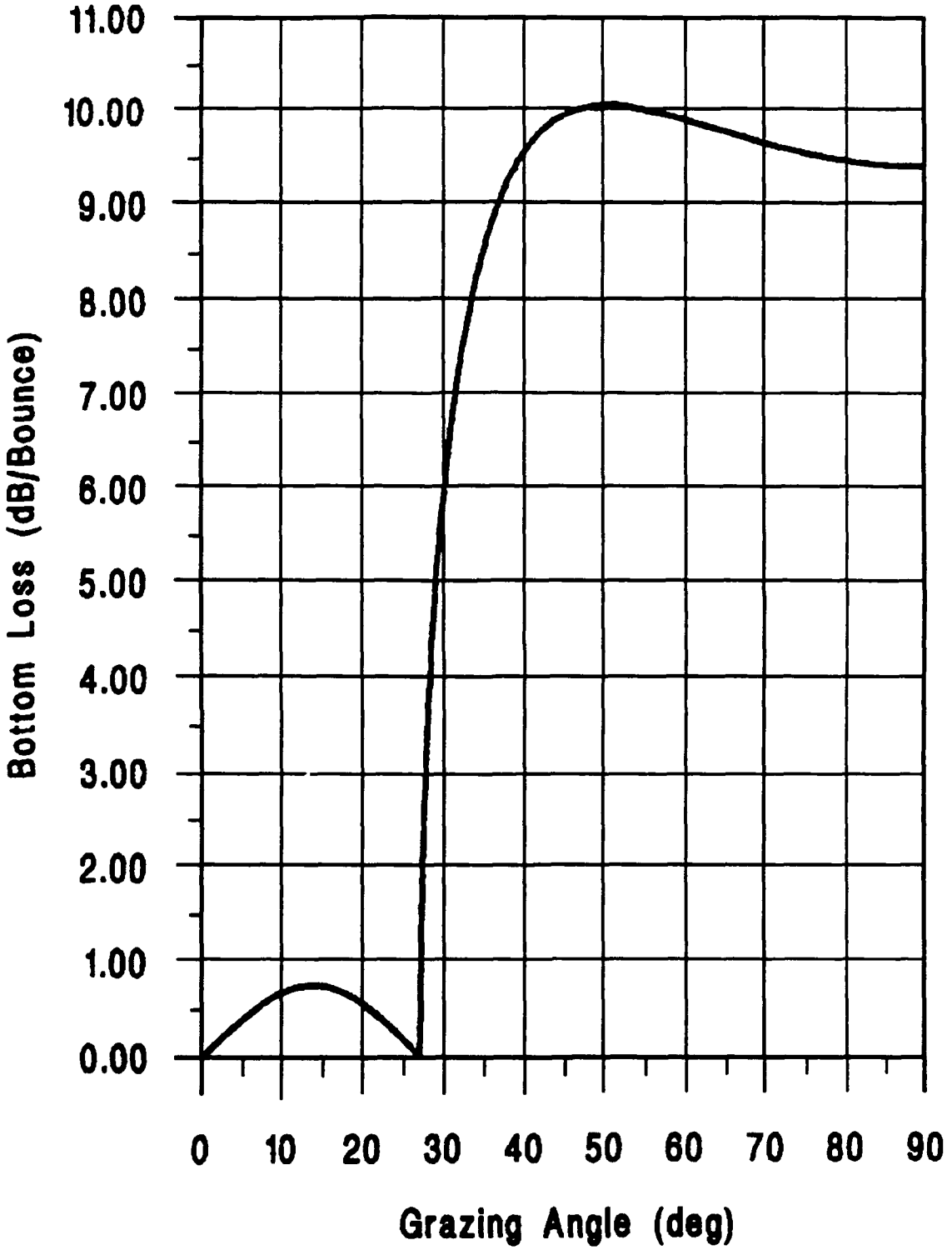

Figure 3.5 Bottom loss vs. grazing angle at 224Hz.

wave length (λ) of the incident ray.

The reflection coefficient at the sea surface can be modeled as a function of wave number (k), rms wave height (σ), and grazing angle (θ) assuming the surface has a Gaussian PDF (Clay and Medwin, 1977):

$$\Re_{sfc} = e^{-2k^2\sigma^2\sin^2\theta} \qquad \text{Eq. 3.2}$$

Figure 3.6 shows the surface reflection coefficient versus grazing angle for angles $0° < \theta < 90°$ for rms wave heights of 0.7071 m (sea state 3) and 2.828 m (sea state 5) respectively.

2. Surface Loss

The surface loss (SLOSS) incurred by the signal at each interaction can be calculated from the reflection coefficient as:

$$\text{SLOSS} = -20 \log (|\Re_{sfc}|) \qquad \text{Eq. 3.3}$$

Figures 3.7 and 3.8 show a plots of SLOSS versus grazing angle for rms wave heights of 0.7071 m and 2.828 m, respectively, at 224 Hz.

Note the effect that sea state has upon SLOSS. At sea state = 3 and $\theta < 30°$ SLOSS is < 2 dB/bounce. For sea state = 5 and $\theta < 30°$, SLOSS is approximately an order of magnitude larger. Thus, at high sea states the loss due to surface interactions of high θ rays would be prohibitively large. However, for small θ SLOSS is small or zero even at the highest sea states because the low angle rays have few or no

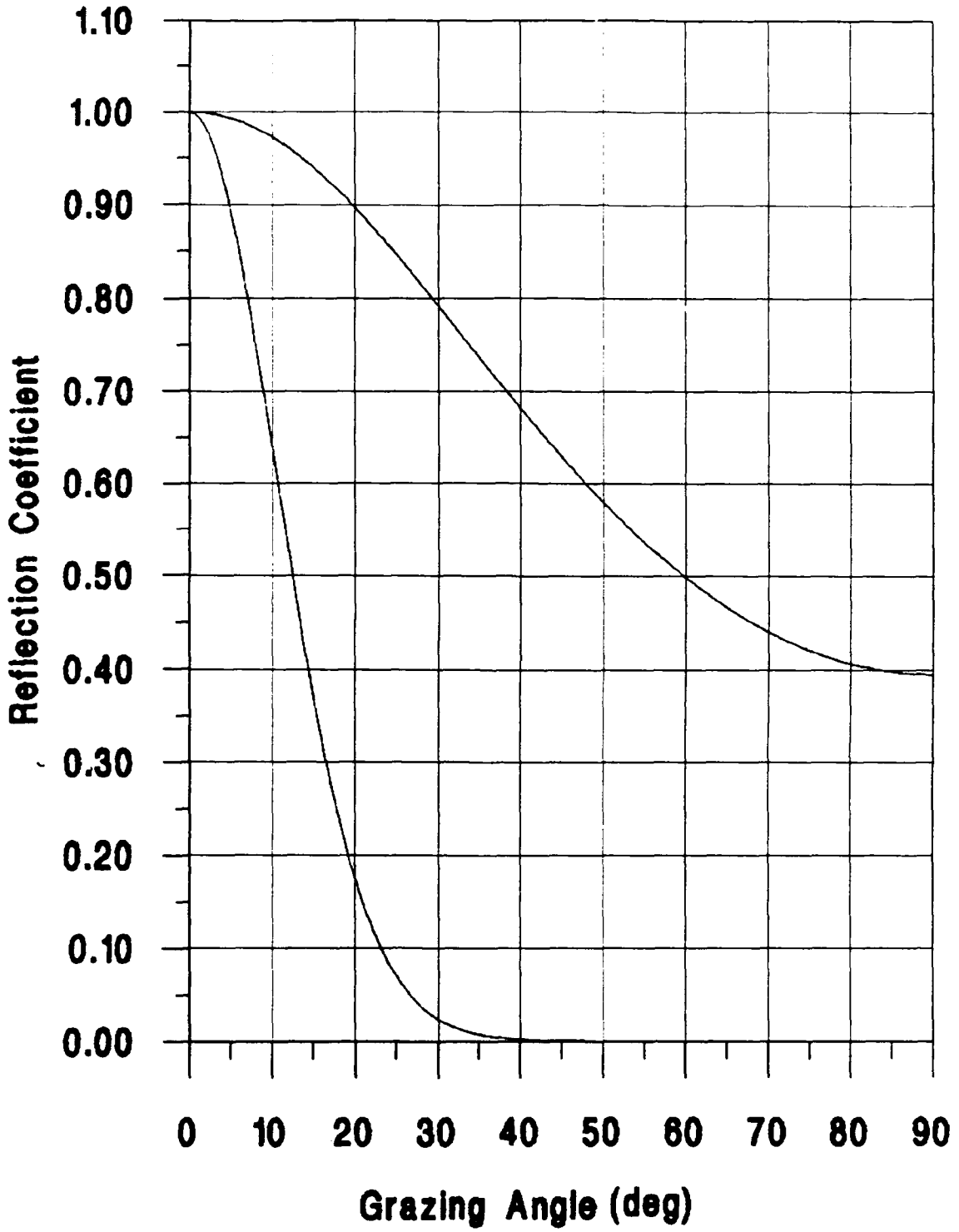

Figure 3.6 Surface reflection coefficient vs. grazing angle for sea states 3 and 5 and frequency of 224 Hz.

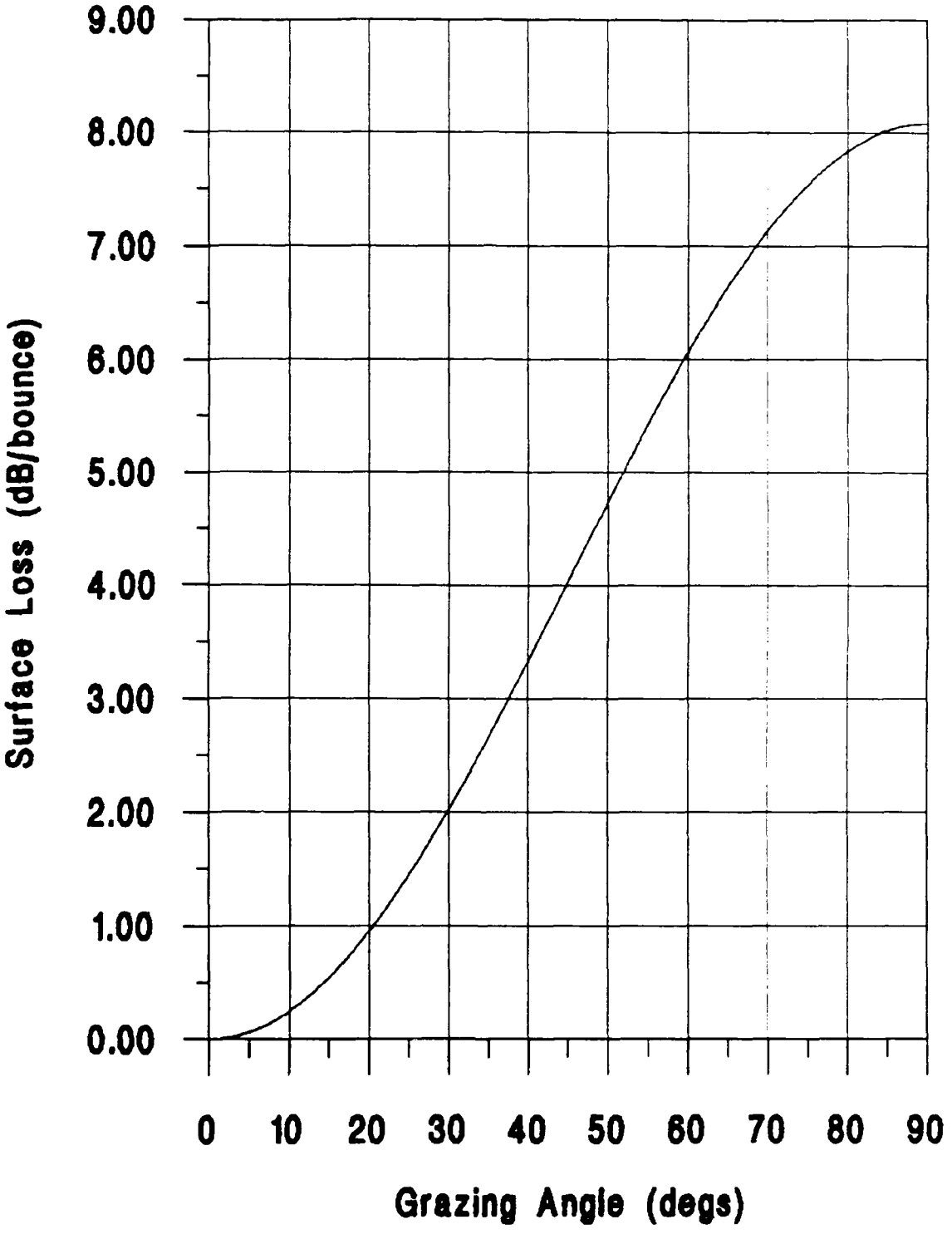

Figure 3.7 Surface loss (dB/bounce) vs. grazing angle for sea state 3 at 224 Hz.

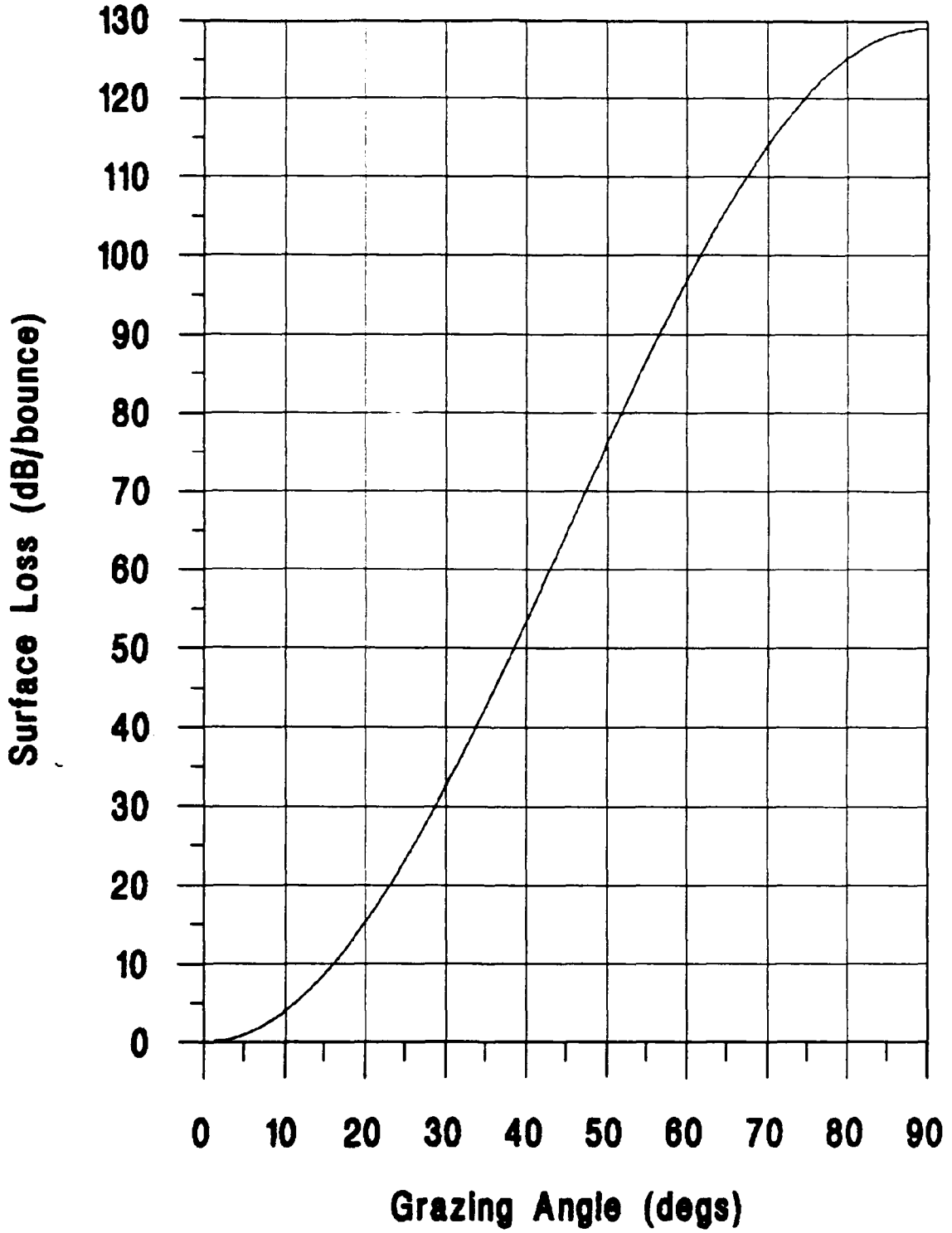

Figure 3.8 Surface loss (dB/bounce) vs. grazing angle for sea state 5 at 224 Hz.

surface interactions as demonstrated by our raytraces. Thus, only in low sea states (< 5) will the high angle rays be receivable. In sea states < 3 the surface loss is essentially zero for all grazing angles, and high elevation rays will be limited only by their number of bottom interactions.

Low launch angle rays have few or no iterations with the surface, as will be discussed in Chapter IV, and will thus have a low value for SLOSS. However high launch angle rays have many surface interactions and will thus have higher values for SLOSS decreasing the value of the SNR as discussed in the rest of this chapter.

D. Sonar Equation

In order to use the signal travel time information for tomographic inverses the transmitted signal must be received with sufficient amplitude so that it is not masked by the noise field. The path that any acoustic signal travels subjects the signal to a variety of loss mechanisms: spreading, scattering, absorption, bottom, and surface losses. Also present in the marine environment are a vast array of noise sources. The received signal must be as loud as the noise level, after signal processing, for it to be useful. The ratio of acoustic signal to environmental noise is calculated as (Kinsler *et al.*, 1982):

$$\mathbf{SNR = SL - TL - LE} \qquad \text{Eq. 3.4}$$

Where: SL = source level (dB re 1μPa @ 1 m)

TL = transmission loss (dB re 1μPa)
LE = directional noise field composed of ambient (L_a), and self (L_e) noise components.

The passive sonar equation can be applied in one form or another to any passive listening system. Each of the terms must be fully evaluated, or estimated, in light of the environmental conditions to determine the optimum source-receiver geometry.

The SL for the sources to be used in the Barents Sea Acoustic Tomography Transmission Test will be 183 dB re 1μPa @ 1 m, and will be transmitted at three different center frequencies[5] (Table 1.1) from three different moorings (Figure 1.1). The TL and LE for Source 1 to the receiving array (Figure 1.1) are calculated in the following sections; similar calculations can be carried out for the other paths and the results should be similar. Table 3.3 summarizes the results of the sonar equation calculation.

1. Transmission Loss (TL)

Transmission loss can be thought of as the sum of the effects of all the factors which remove acoustic energy from a transmitted signal: spreading, bottom interactions, surface interactions, volume scattering, and absorption. The values for spreading loss are calculated by HARPO and are elevation

[5] The SL used here is band level, not spectrum level. LE and SNR discussed below will be corrected for signal band width to make them spectrum levels also.

angle dependent due to the differences in path length of the different rays. Absorption is also calculated by HARPO but is negligible. Thus, TL can be calculated as:

$$TL = \text{Spreading} + BL + SLOSS \qquad \text{Eq. 3.5}$$

Using a separation range of 75 km, the TL from S1 to R1 (Figure 1.1) for signals propagating along rays of various launch angles was calculated. Table 3.1 shows the various components of TL, and the TL for rays of elevation launch angles of 10°, 15°, 16°, 17°. Table 3.2 displays the numbers of surface and bottom interactions used to calculate the losses for each of the 4 rays in Table 3.1. Note that the TL for rays 17° and higher is greater than the source level. Therefore, rays launched at angles above 17° will be attenuated before they reach the receiver in high sea state situations. However, if the sea state is very low, then SLOSS

TABLE 3.1 TL Components for 0.7071 m Wave Heights.

Elevation Angle	10°	15°	16°	17°
Spreading Loss	91.4	90.6	86.2	91.9
Surface Loss	0.24	4.87	18.41	44.84
Bottom Loss	13.3	17.8	21.0	23.6
TL	104.95	113.31	126.00	160.35

TABLE 3.2 Numbers of Surface and Bottom Interactions for the rays in Table 3.1.

Elevation Angle	10°	15°	16°	17°
Bottom Bounces	1	9	22	30
Surface Bounces	21	23	21	29

decreases significantly and higher elevation rays can be received.

2. Noise Components (LE)

The masking noise field in the ocean environment derives from many sources that can be grouped into two categories, ambient (La) and self noise (Le). La includes contributions from shipping, agitation of the sea surface, bioacoustics, sea ice, and seismic sources. Le is the noise added to the received signal by the receiving platform or ship. LE is calculated by a power summation of La and Le.

Le varies from ship to ship and with speed of the ship, and also covers the entire spectrum of sound from VLF to UHF. The ship scheduled to be used for the Barents Sea Acoustic Tomography Transmission Test is the *USNS Bartlett* for which NAVOCEANO has no specific noise data. However, ships of similar size and configuration have demonstrated a spectrum source level of 120 dB re $1\mu Pa^2/Hz$ in the band 200 to 250 Hz (Reynolds, 1991), and this number will be used as

representative for the *Bartlett*. Assuming this noise source radiates spherically, the transmission loss is 60.0 dB at a standoff distance of 1 km from the receiver array making L_{self}=60 dB. Correcting L_{self} for the band width of the 224 Hz signal, 16 Hz, raises L_{self} to 72 dB.

As stated above, La has several components. L_{ice} is an order of magnitude less than the other components of La due to the large distance to the expected ice edge (Figure 2.2) and is ignored here. Bioacoustic noise is also not considered here. Shipping noise (L_{ship}) is composed of the noise added to the environment by distant shipping. Figure 7.5 in Urick (1977) plots the spectrum level of L_{ship} for high, medium and low shipping-density areas. By assuming a medium shipping density of the Barents Sea in summer, the peak of the fishing season in the region, L_{ship} is found to be 51 dB, at 224 Hz, which corrected for the 16 Hz band width increases to 63 dB.

The noise due to the agitation of the sea surface (L_{ss}) increases as wave height increases due to increasing wind speed. At 224 Hz and mean wave height of 1 m L_{ss} is 68 dB, for a 4 m wave height L_{ss} is 73 dB. These values must be corrected for band width as before and the corrected values are shown in Table 3.3.

Table 3.4 summarizes the inputs to the sonar equation and the resulting SNR values for rays launched at 10°, 15°, 16°, 17° and a source/receiver separation of 75 km. The SNR values

TABLE 3.3 Components of LE at 224 Hz. Noise levels have already been corrected for the band width of the 224 Hz signal.

Sea state/Mean wave height (m)	3/1	5/4
L_{ss}	80	85
L_{ship}	63	63
L_{self}	72	72
LE	81	85

in Table 3.4 demonstrate that at elevation angles above 17° the rays suffer so much TL that even with signal processing gains of 40 dB the signal will not heard above the noise. The TL values in Tables 3.1 and 3.4 are conservative estimates due to ignoring contributions to the acoustic path from energy refracted through the layered sediments.

TABLE 3.4 Sonar Equation Summary for sea state 3. All acoustic units dB re 1μPa.

Elevation Launch Angle	10°	15°	16°	17°
SL	183	183	183	183
TL	104.95	113.31	126.00	160.35
LE	81	81	81	81
SNR	-2.95	-11.31	-24.00	-58.35

IV. ACOUSTIC RAYTRACING

Ray theory allows for the simulation of acoustic rays through a medium whose refractive index structure can vary in a complex manner (Ort, 1991). Raytracing provides a visual representation of the paths taken by sound energy through the medium and graphically illustrates how various ocean structures affect the arrival of each ray.

The three-dimensional raytracing program HARPO (Hamiltonian Acoustic Raytracing Program for the Ocean) is used for this study because it provides a method for dealing with the sound speed and bathymetric structure in a continuous manner. Because of its continuous treatment of the problem HARPO overcomes the many problems suffered by earlier raytracing routines such as false caustics and discontinuous rays (Jones *et al.*, 1986). Ray theory assumes conservation of energy within a bundle of rays. If the cross sectional area of a bundle goes to zero a caustic is produced and ray theory predicts infinite energy density at that point. Methods of correcting ray theory near caustics are discussed in detail by Brekhovskikh (1980).

A. Hamiltonian Ray Tracing

Rays can be traced by integrating a differential form of Fermat's principle, i.e., Hamilton's equation (Jones *et al.*, 1986). In the high frequency limit waves behave like particles and travel along rays. Therefore, Hamilton's equation governing changes of position and momentum in mechanical systems can also be applied to sound propagation at high frequency (Lighthill, 1978). Hamilton's equation has the general form:

$$\frac{dp_i}{dt} = \frac{\partial H}{\partial q_i} \qquad i=1,..3$$
$$\frac{dq_i}{dt} = \frac{\partial H}{\partial p_i} \qquad i=1,..3 \qquad \textbf{Eq. 4.1}$$

where $H(p_1, p_2, p_3; q_1, q_2, q_3)$ is a Hamiltonian function describing the total energy of a system in terms of a generalized coordinate system p and momenta q. For acoustic application q is the wave number vector $(\vec{k})$ and p is a coordinate system $(\vec{x})$. In HARPO the coordinate system is spherical polar. Solutions to Eq. 4.1 for ray paths in the ocean are obtained by choosing initial values for the six values of k_i and x_i [6] and integrating this system of six differential equations. For sound propagation in the ocean the Hamiltonian takes the form:

---

[6] k_1 and k_2 are the horizontal wave number components and k_3 is the vertical component. x_1 and x_2 define the horizontal position and x_3 the vertical position.

$$H(x_i, k_i) = \omega^2 - c^2(x_i)k^2 = 0 \qquad \text{Eq. 4.2}$$

where $c(x_i)$ is the sound speed field and ω is the angular wave frequency (Jones, *et al.*, 1986).

B. HARPO OVERVIEW

HARPO is an algorithm for raytracing that numerically integrates Hamilton's equation. It allows for a continuous three-dimensional representation of the refractive index field, and a two-dimensional representation of the upper and lower reflecting surfaces. Also HARPO permits a trade off of speed for accuracy by manipulation of allowable single step integration error[7]. Hence the results can either be fast and crude or slow and more accurate.

Input fields to HARPO are constructed by a combination of subroutines. These subroutines generate analytical, canonical models of currents, bathymetry, sound speed, absorption, and perturbations to each of these. By including a velocity vector to model motion of the fluid medium in the Hamiltonian (Eq. 4.2) the effects of ocean currents can be included. Ocean currents will not be modeled in this study. These subroutines may be combined as needed by the user to create a simulation of real world conditions that are of interest to

[7]The allowable single step integration error determines how close HARPO will come to the actual answer. Large allowable errors allow the program to run faster, and small allowable errors cause the program to run slower as it works towards a more exact answer.

the study being conducted. In addition to the original subroutines, Woods Hole Oceanographic Institution (WHOI) and the Naval Postgraduate School (NPS) created a set of new subroutines for HARPO that allow for the input of discretized bathymetry and sound speed fields. These discretized fields are made continuous by the use of empirical orthogonal functions (EOFs) and splines to meet the input requirements of HARPO, i.e., continuous derivatives, first order in the case of sound speed, and second order for bathymetry (Newhall *et al.*, 1987).

The ocean represented by the inputs to HARPO must be deterministic, not random, because HARPO's computations apply no corrections for diffraction or partial reflection (Jones *et al.*, 1986). HARPO makes no reality checks of the representations used to define the ocean and will allow geostrophically inconsistent current and sound speed models to coexist. Therefore, care must be taken to ensure that the input ocean variables are physically realistic.

HARPO also makes no attempt to compute the amplitude for the signal at any point along a ray. Amplitude calculations can take on several different forms, but none have any effect upon the ray path and as such they are left to external programs applied to the machine readable or ASCII HARPO output files. HARPO also makes no attempt to find eigenrays[8]; these

[8]Eigen rays are those rays that directly connect the source with the receiver.

rays are easily derived from the RAYSET output of HARPO by use of external programs (Jones *et al.*, 1986). For a complete description of the mathematics and coding of HARPO the reader is referred to the documentation of HARPO by Jones *et al.* (1986).

C. Modeling The Barents Sea

Chapter II described the oceanographic environment of the Barents Sea. Modeling this environment for acoustic ray analysis was accomplished by selecting a set of computer routines and environmental data that provided an adequate mathematical description for the sound speed field and bathymetry. The accuracy with which HARPO calculates ray paths is dependent upon the accuracy with which the ocean is described by the model. Early runs of HARPO demonstrated a need to filter the input sound speed profiles to remove fine structure perturbations (less than a wavelength in size) in the vertical because they were causing physically unreal rays to be traced. This was necessary because ray theory is an infinite frequency approximation, which implies that the results are sensitive to fine scale perturbations. In actuality we were using a finite frequency of 224 Hz. For the low frequency experiment being modeled, the existence of fine structure in the sound speed profile could be safely ignored.

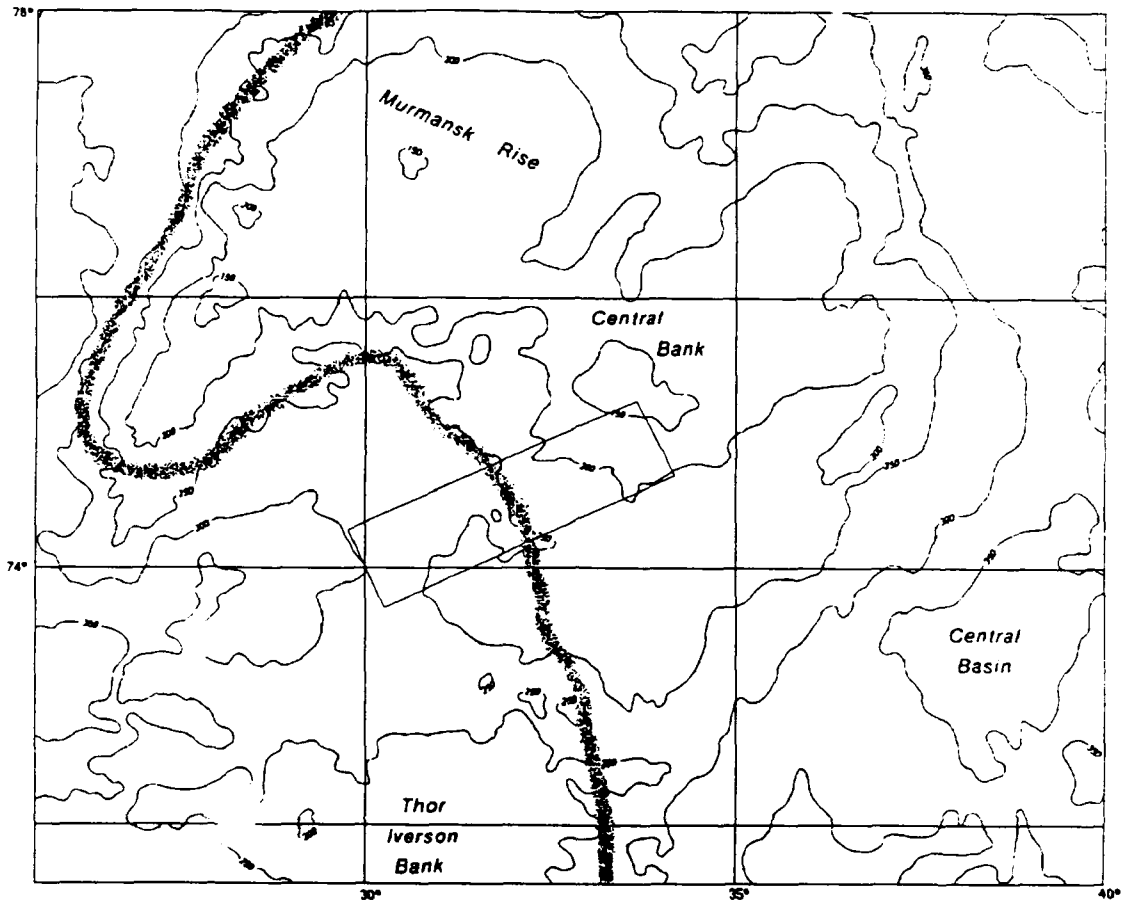

Figure 4.1 Bathymetric details (after Cherkis *et al.*, 1990) and mean position of the Polar Front (after Loeng, 1991).The box marks bathymetric area for HARPO.

Figure 4.1 shows the geographical limits of the modeled ocean used in this ray analysis. Unclassified data on the sound speed, temperature, and salinity fields are sparse in the Barents Sea. The NAVOCEANO MOODS database is one of the few unclassified databases that does contain a number of CTD casts in the Barents Sea, many taken from the R/V Vema and USNS Kane cruises during the summers of 1986 and 1987.

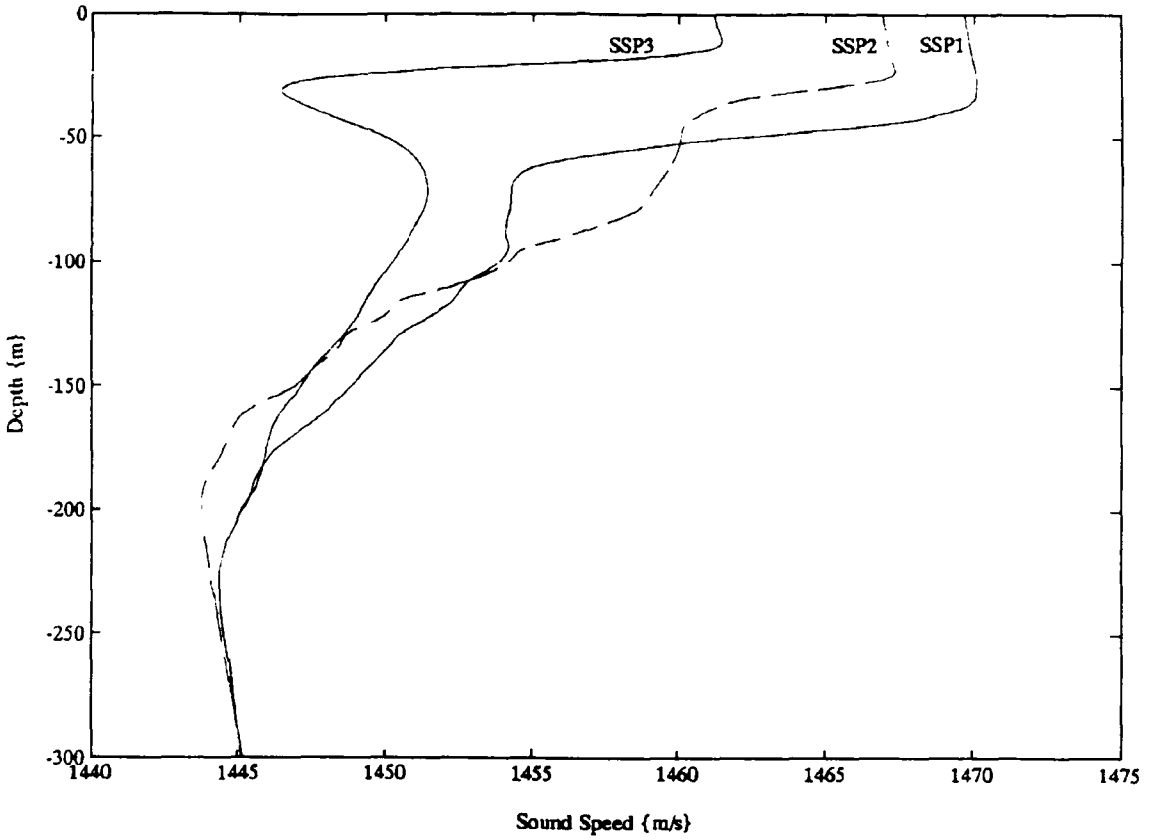

Figure 4.2 Three sound speed profiles representative of NAW (SSP1), PW(SSP2), and AW(SSP3) in the Barents Sea in August.

1. Sound Speed and Bathymetry Fields

The creation of the input sound speed field for HARPO was an iterative process. Figure 4.2 shows the three sound speed profiles (SSPs), extracted from the NAVOCEANO MOODS database, chosen to represent conditions on the North Atlantic side of the Polar Front(SSP1), front interior front(SSP2), and on the Arctic side(SSP3), respectively (Figure 4.1). From SSPs above five others were created by interpolation to smooth the sound speed field on each side of the front (Figure 4.2). The five new profiles and the three original profiles are distributed

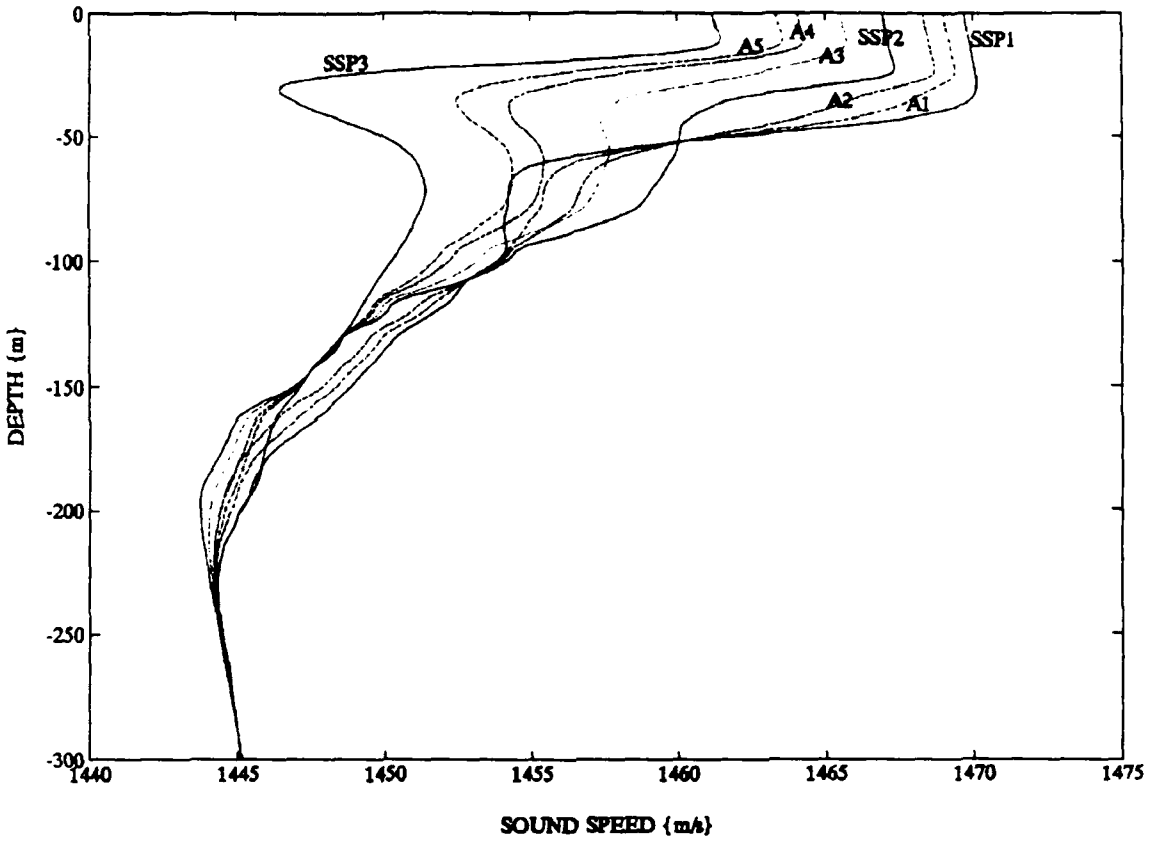

Figure 4.3 Sound speed profiles created by an interpolation between the measured profiles (SSP1, SSP2, and SSP3) for model cases 1 and 2.

over the 75 km path length and are used in the first two model runs to be described later (Figure 4.3). For the third model case SSP3 and SSP1 were used to create six SSPs distributed over the 75 km path length by linear interpolation (Figure 4.4).

The bathymetry input to HARPO is shown in Figure 4.1. The rectangular box was gridded into 20 subdivisions along the long sides, and 10 subdivisions along the shorter sides. The bottom depths were then manually read off the chart and input to HARPO via one of the WHOI/NPS HARPO subroutines.

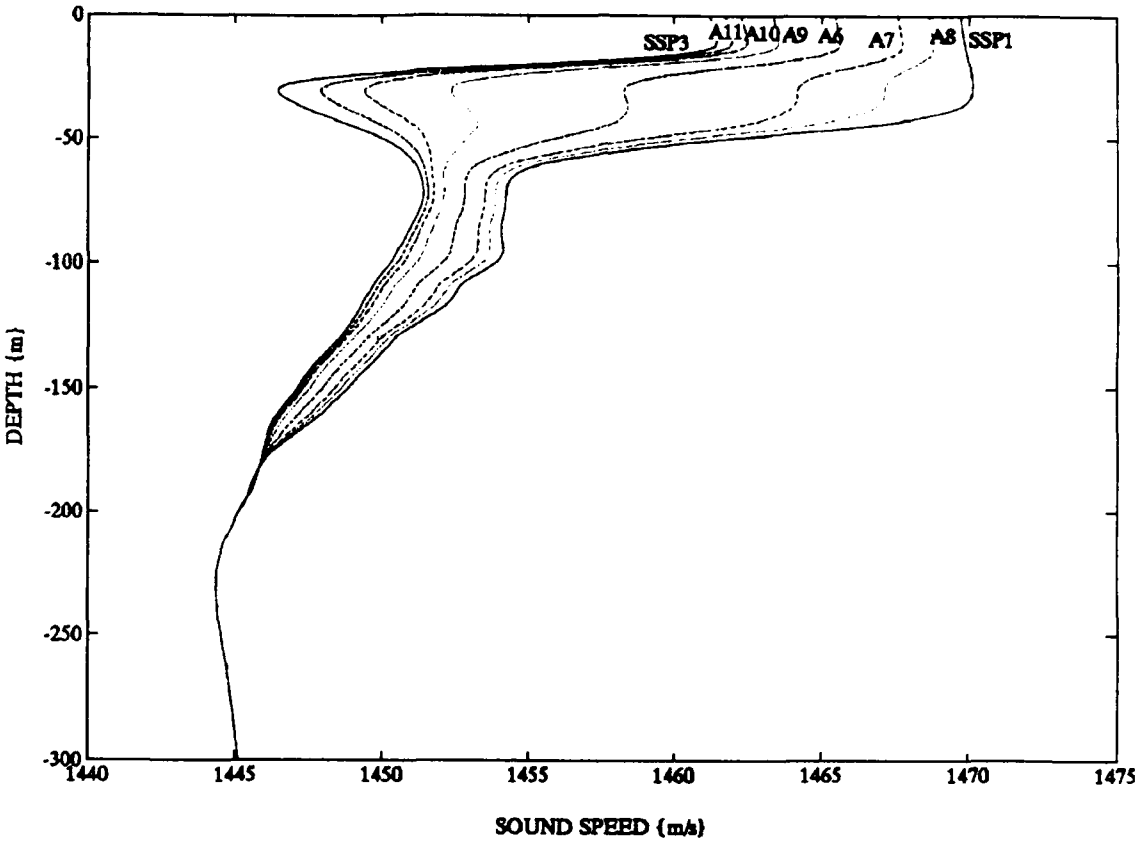

Figure 4.4 Sound speed profiles created by a linear interpolation between the measured profiles (SSP1 and SSP3) for model case 3.

2. Other HARPO inputs

Aside from the sound speed and bathymetric inputs HARPO requires models to describe the sea surface and its perturbation and sea water absorption and its perturbation. The sea-surface was modeled as a sphere concentric with the earth with no perturbation. The absorption of acoustic energy by the sea was modeled by HARPO using the method of Skretting and Leroy (1971). This method is dependent only upon acoustic angular frequency with the absorption coefficient given by

$$\alpha = a\left(\frac{\omega^2}{\omega_1^2}\right) + b\left(\frac{\omega^2}{\omega_2^2+\omega^2}\right) \qquad \text{Eq. 4.3}$$

where:

$$a = 0.006 \text{ dB/km}, \quad b = 0.2635 \text{ dB/km}$$
$$\omega_1 = 6283.2 \text{ rad/s}, \quad \omega_2 = 10,681.4 \text{ rad/s}$$

and no perturbation was applied.

D. Results

1. HARPO runs

HARPO was run for three different sound speed fields (Table 4.1) each designed to describe possible conditions in the Barents Sea during the summer. The first field was used to represent a situation where the source is in North Atlantic Water (NAW), the receiver is in Arctic Water (AW) and a mixed Frontal Water (FW) is in between. The second field was used to represent a condition where the source is inside the FW and the receiver is in AW. The third field was used to represent a situation where the source is in NAW and the receiver in AW and no defined front exists between them. The last situation models a weak, diffuse front which is possible in the Barents Sea in the region of the study.

To examine the impact of the front and the strong vertical gradient associated with NAW on propagation from a near-bottom sound source ray traces were constructed for launch angles of 6°, 10°, and 15° (Figure 4.5). At these launch angles the rays are refracted from the underside of the thermocline and hence

TABLE 4.1 Description of the Source/Receiver and Frontal positions for the three model cases.

CASE No.	SOURCE LOCATION	RECEIVER LOCATION	FRONT LOCATION
1	74.25°N 32.2°N	74.4°N 34.8°E	BETWEEN SOURCE AND RECEIVER
2	74.25°N 32.2°N	74.4°N 34.8°E	INCLUDES SOURCE
3	74.25°N 32.2°N	74.4°N 34.8°E	NO DEFINED FRONT

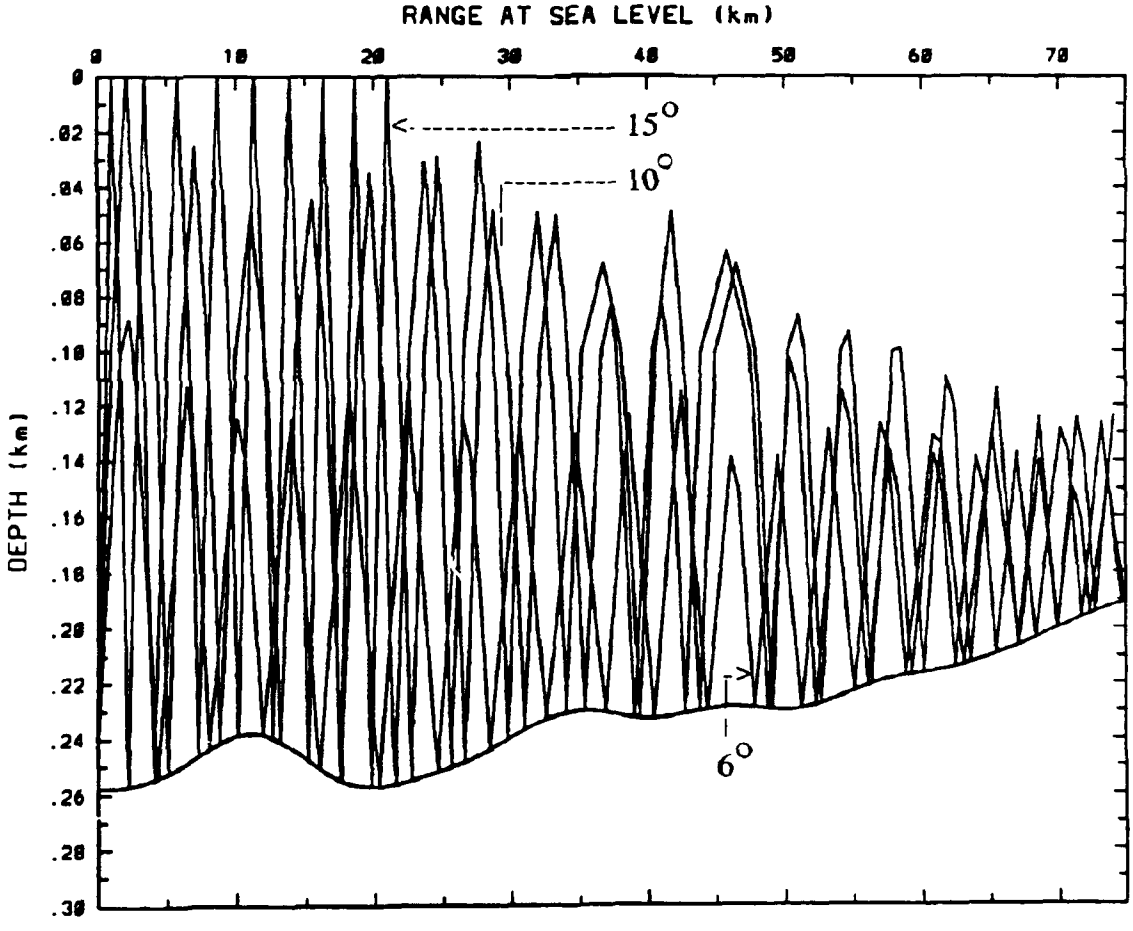

Figure 4.5 Raytraces for elevation angles of 6°, 10°, and 15° for all three model cases.

they give information about the vertical extent of the frontal feature. The 6° ray is a *refracted bottom-reflected* (RBR) ray, the 10° ray has one surface reflection and is RBR the rest of its path, and the 15° ray starts as a *surface-reflected bottom-reflected* (SRBR) ray, but changes character to an RBR ray as the influence of the Arctic Water changes the refractive index of the medium to such an extent that the rays are turned prior to reaching the surface. Only one plot for these three rays is presented here, since the differences in ray paths caused by varying the frontal characteristics are not readily visible due to the scale of the plot. However, the differences are observable by examining the arrival times of the rays for each of the frontal locations.

Figure 4.6 shows a raytrace for a launch angle of 17.7°. Note that for launch angles higher than 16.2° the rays are SRBR. The differences between raypaths for rays launched at 17.7° or higher, for any of the frontal positions, are again not visible. The small size of path variations due to the different frontal representations indicates that the acoustic arrivals are stable in the presence of mesoscale ocean perturbations.

2. Arrival time structure

Examination of the arrival times of the acoustic rays reveals information about the resolvability, duration of pulse response, and oceanographic signal strength of the system.

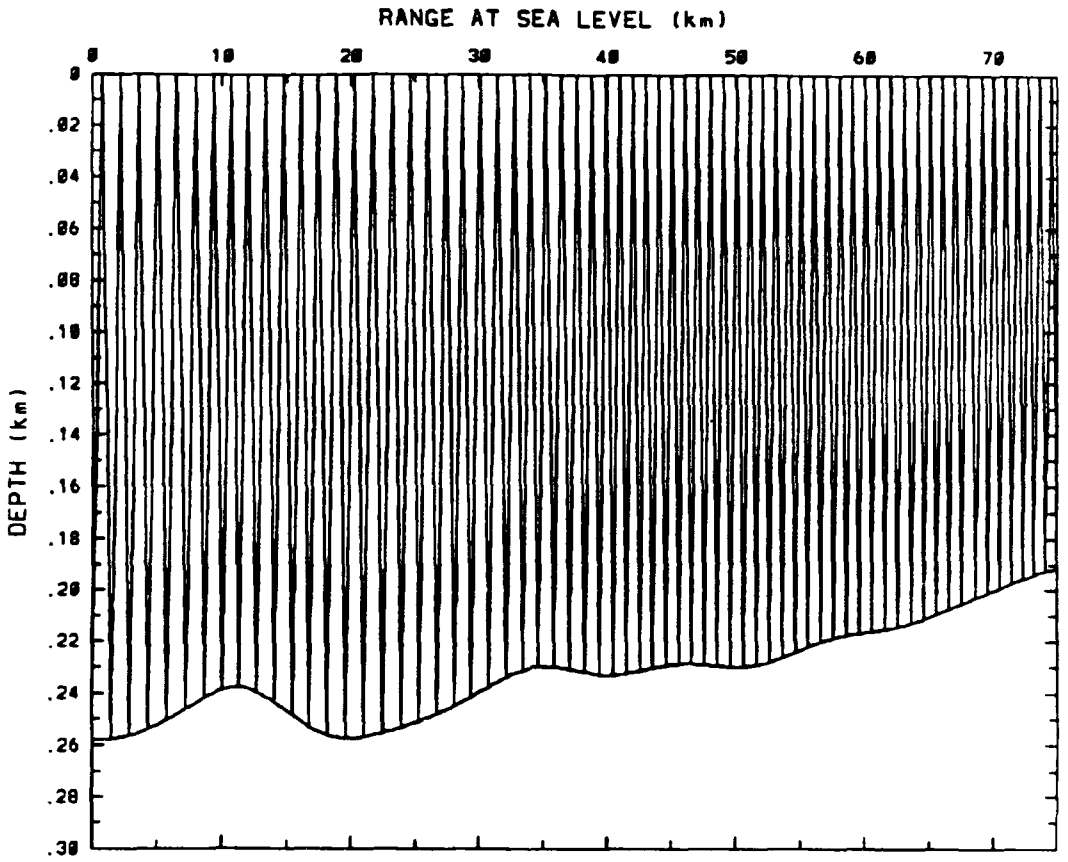

Figure 4.6 Raytraces for elevation launch angle of 17.7°.

To accomplish this examination rays from 0° to 25° at 0.1° intervals were constructed for a near-bottom source (250 m depth) to a vertical receiving array 75 km away. Eigenrays were taken to be any ray which completed the 75 km path with ≤ ±1 m of horizontal deviation. Conclusions about the feasibility of conducting acoustic tomography in this environment are based upon those rays that complete the entire 75 km range, and the SNR of those rays as discussed in the previous chapter. Rays launched in the range from 0° to 5° are not of interest because they are all scattered out of the line

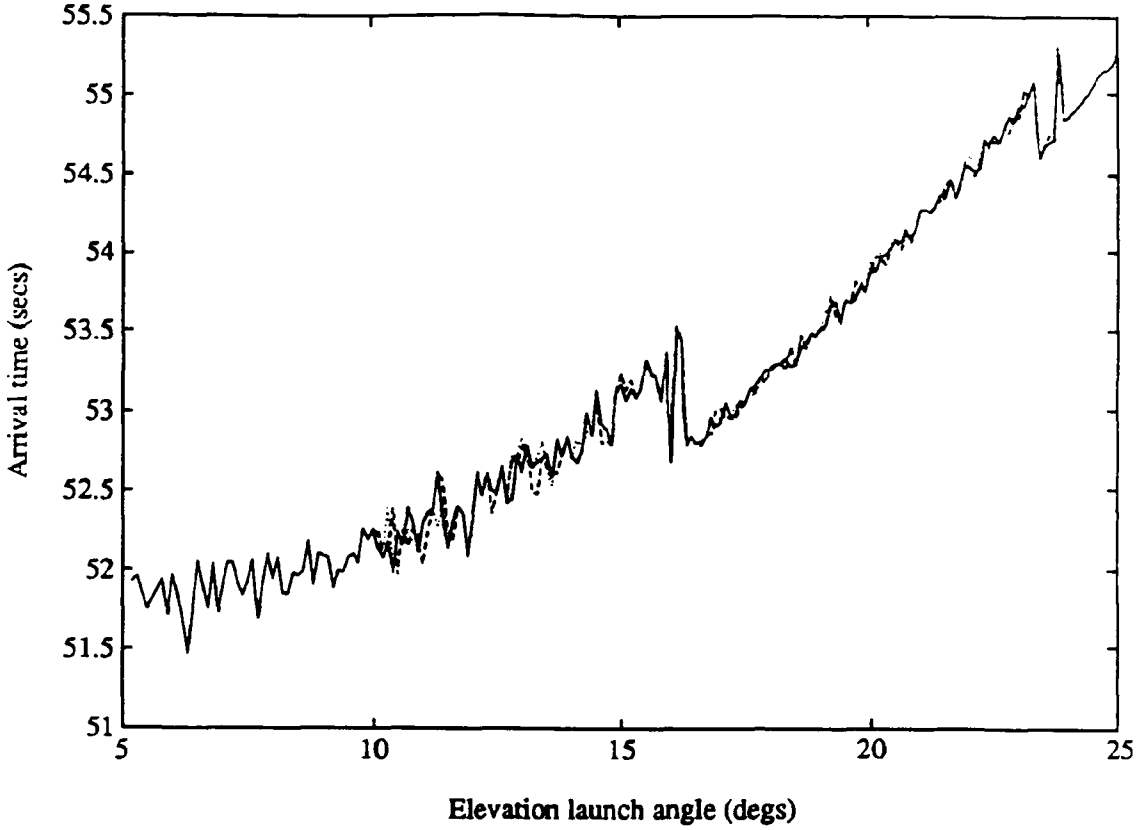

Figure 4.7 Arrival time vs. elevation launch angle for angles from 5° to 25°. The solid curve is for model case 1, dashed for case 2, and dotted for case 3.

of sight by bottom interactions before they complete the 75 km range.

The arrival time versus launch angle for angles between 5° to 25° is shown in Figure 4.7 for each of the 3 model cases. The range of launch angles shown in this figure can be broken up into 2 regions for evaluation, 5°-17° and 17°-25°. These two regions describe two distinct parts of the spectrum of arrivals which pass through different parts of the medium. Rays launched at < 17° mostly contain information about the horizontal variation of the vertical extent of the front.

Rays launched at > 17° mostly contain information about the interior structure of the front.

In the range 5° to 10° (Figure 4.7) all three frontal situations give the same path lengths, and thus arrival times are exactly the same in all three cases. This is because these rays are RBR rays and stay in the deepest 50 to 70 m of the water column where the SSPs are the same for all three frontal characteristics examined (Figures 4.3 and 4.4).

Figure 4.8 shows the time of arrival for elevation angles from 10° to 15°. Rays launched in this range generally are not surface interacting but are RBR rays. In the range from 10° to 17° the first differences in arrival time become evident. These can be seen in an expanded plot of Figure 4.7 where the interval 10° to 15° is shown as in Figure 4.8. These differences arise from the interaction of the rays with the spatially varying refractive index field of the shallow and mid depth portions of the water column. Faster arrivals, at a particular launch angle, indicate that the ray path is passing through higher speed layers as a result of changes in the frontal characteristics and conversely.

In general the rays in the 5°-17° range reveal information about the horizontal distribution of the vertical extent of the front and about the homogeneity of the deep sound speed structure. Differences in arrival times in this region of Figure 4.7 are due to differences in the position and strength of the front in the horizontal. The fact that only small

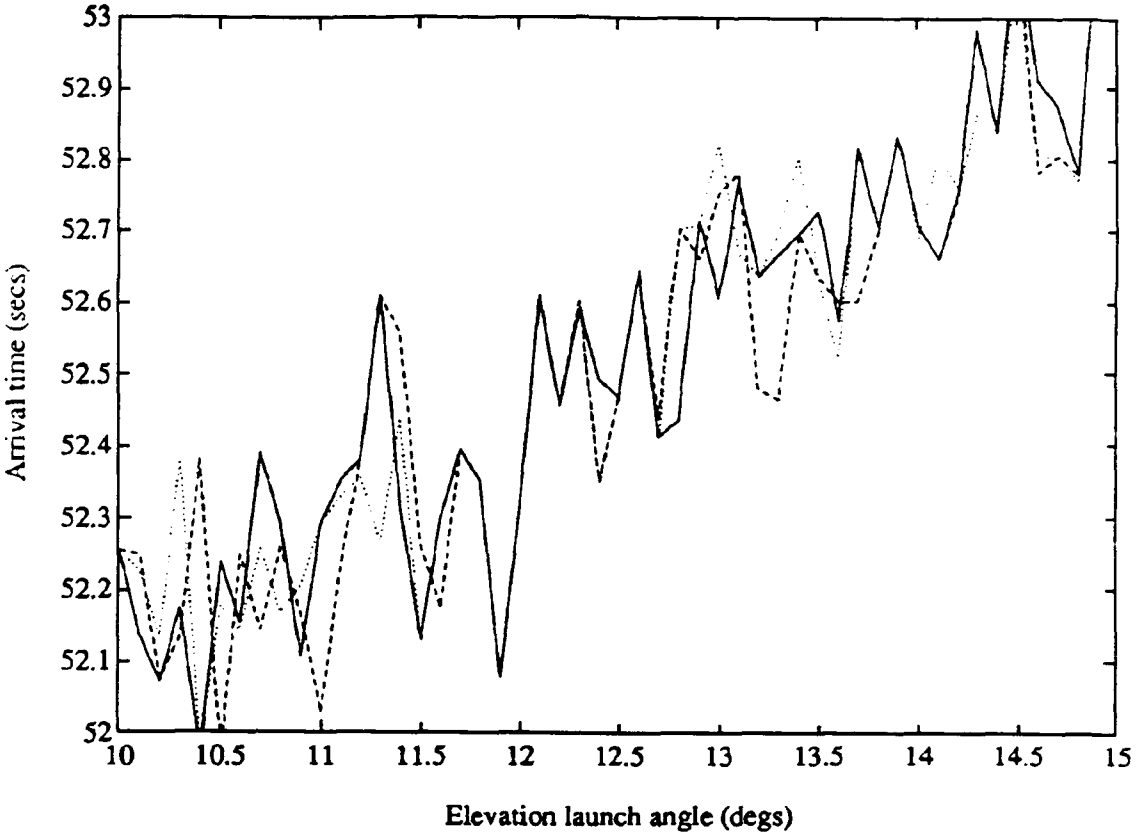

Figure 4.8 Arrival time vs. elevation launch angle for angles from 10° to 15°. Case 1(Solid), Case 2(Dashed), Case 3(Dotted).

differences exist between the cases demonstrates the stability of the system in the presence of frontal oscillations.

Rays at angles greater than 17° reveal information about the interior structure and horizontal extent of the front. Differences in travel time in this range arise from sound speed and path length differences, the latter being caused by the thickness of the front. The wider the front the longer the path length and travel time. The converse is also true.

In both ranges of launch angles the differences in arrival time between the cases reveal the oceanographic signal strength of the modeled Polar Front (Figure 4.7). The fact

that significant travel time differences of 50 to 100 ms exist between the three cases demonstrates the observability of frontal oscillations.

3. Eigenray arrival structure

Figure 4.9 shows the curves of depth versus launch angle for all three model cases. The number of eigenrays that arrive at any particular depth at the receiver location 75 km

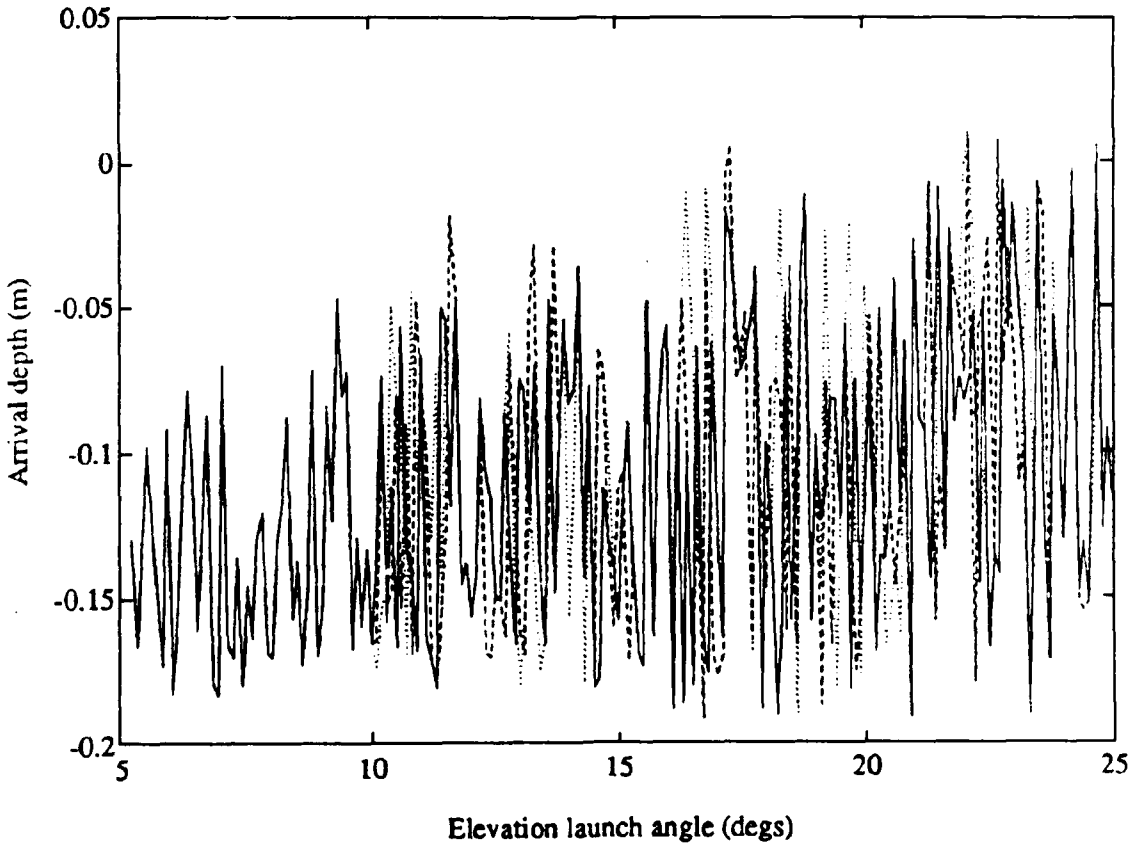

Figure 4.9 Curves of arrival depth versus elevation launch angle. The solid curve is for model case 1, dashed is for case 2, and dotted for case 3.

away, can be found by drawing a horizontal line across Figure 4.9 at that depth. Eigenrays are given by the intersections with the curve associated with each model case.

The ray arrival structure for a hydrophone located at mid-column depth (100 m) is shown in Figure 4.10. In this plot eigenray arrival times against received angles are displayed. Received angle is the angle a ray makes at the receiver (< 0° indicates an upward traveling ray, while >0° indicates a downward moving ray). It is seen from Figure 4.10 that many

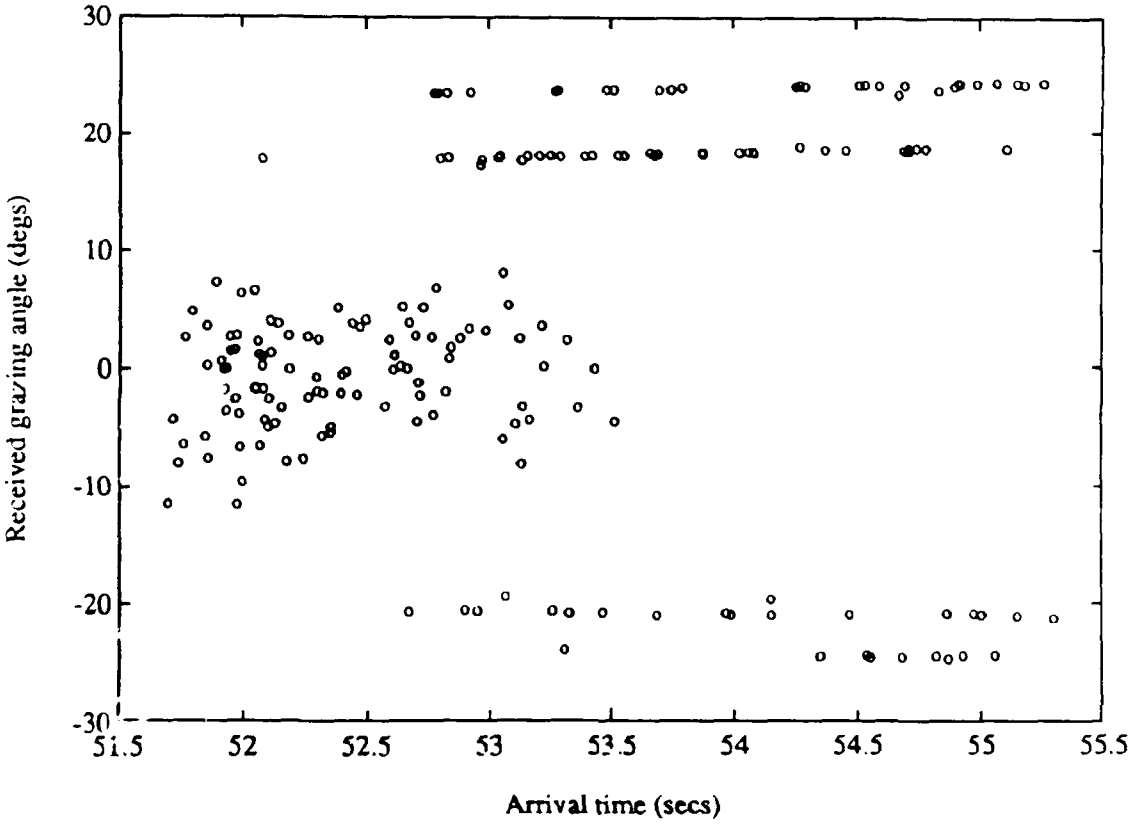

Figure 4.10 Eigenray arrival times vs. receiving angle at the receiver plane for model case 1 at mid-column depth (100 m).

ray arrivals are resolvable for mid-column hydrophones with a beam forming capability since most arrivals do not come at the same time and angle.

At depths near the bottom of the water column many more overlapping arrivals are observed in compared to the mid-column depths. This complex structure of arrivals may require a modal examination to provide resolvability.

V. CONCLUSIONS

The objectives for this thesis were to examine the physical oceanography of the Barents Sea, and to evaluate, in numerical experiments, the feasibility of using ocean acoustic tomography for frontal monitoring in the Barents Sea.

The following are a few highlights of the Barents Sea oceanographic environment:

1. The Barents Sea is probably the least well explored of any sea in the world that is not constantly ice covered.

2. Major oceanographic feature is the Barents Sea Polar Front, separating NAW and AW.

3. The literature contains little to no information regarding the precise location of the Barents Sea Polar front from year to year and season to season with the exception of the region around Bear Island (Johannssen and Foster, 1978).

4. The location of the Barents Sea Polar Front from year to year is a strong function of the previous spring's Norwegian Sea cyclonic storm activity. A strong storm season brings a large amount of warm NAW into the Barents Sea, causing an emptying of the BW from the Central Basin and a subsequent warming of the entire Barents Sea. This results in a sea ice minimum to be generated the following year. The periodicity of this event is on the order of 6 years (Blindheim and Loeng, 1981) and last occurred in 1989 (Loeng, 1991).

5. The bottom sediment conditions are stable throughout the Barents Sea due to very slow sedimentation rate. This results in stable bottom acoustic conditions from year to year and season to season.

The feasibility of conducting a tomographic exercise is best discussed by an examination of eigenrays. This study

examined those rays that intersected a vertical plane 75 km from the source. Conclusions based upon those rays, and in general the entire rayset, are:

1. The ray paths are stable in the presence of frontal oscillations.

2. The duration of multipath arrival structures is about 3 to 4 seconds. Therefore, the longest pulse code transmission will have to be < 3 secs.

3. Ray arrivals are resolvable for mid column hydrophones, but may not be resolvable for hydrophones close to the bottom. For near-bottom hydrophones modal techniques may be needed.

4. For mean wave heights of 1 m little signal is expected from rays launched at $\geq 17°$.

5. Ray travel time differences (δt) of $\approx$ 50 to 100 ms are expected due to frontal oscillations.

LIST OF REFERENCES

Backus, G.E. and J.F. Gilbert, Numerical application of a formulation for geophysical inverse problems, Geophys. J. Astron. Soc., 13, 247-276, 1967.

Baturin, D.G., and A. UY. Yunov, The evolution of the Barents Sea Shelf as a part of the Geological Development of the Arctic Region. Naval Technical Intelligence Center translation no. 900215, 101-111, 1990.

Blindheim, J. and H. Loeng, On the variability of the Atlantic influence in the Norwegian and Barents Seas, FiskDir. Skr. Ser. HavUnders., 17, 161-189, 1981.

Bourke, R.H., Department of Oceanography Naval Postgraduate School, Monterey, CA., Personal communication, 1991.

Brekhovskikh, L.M., Waves in Layered Media, Academic Press, San Diego, CA, 1980, pp503.

Clay, C.S. and H. Medwin, Acoustical Oceanography, John Wiley & Sons, New York, 1977.

Central Intelligence Agency, Polar Regions Atlas, 1978.

Chavanne, J., Die Eisverhaltnisse in Arkischen Polarmere und ihre periodischen Veranderungen. Geographie und Erforchung der Polar Regionen, 108, 134-142, 245-280, 1875. (In German)

Cherkis, N.Z., H.S. Fleming, M.D. Max, M.F. Czarnecki, Bathymetry of the Barents and Kara Seas(Chart), Naval Research Laboratory, Washington, D.C., 1990.

Chiu, C.S., Department of Oceanography Naval Postgraduate School, Monterey, CA., Personal communication, 1991.

Chiu, C.S., J.F. Lynch, and Ø.M. Johannessen, Tomographic resolution of mesoscale eddies in the MIZ - a preliminary study, J. Geophys. Res., 92(7), 6886-6902, 1987.

Dickson, R.R., L.S. Midttun, and A.I. Mukhin, The hydrographic conditions in the Barents Sea in August-September 1965-1968, in International O-Group fish Survey in the Barents Sea cooperative research report ser. A, no. 18, edited by O. Dragesund, International Council for the Exploration of the Sea, Charlottenlund Slot, Denmark, 3-24, 1970.

Dunn, D., Code OWS, Naval Oceanographic Office, Stennis Space Center, MS, Personal communication, 1991.

Eldholm, O. and J. Ewing, Marine geophysical survey of the southwestern Barents Sea, J. Geophys. Res., 76, 3832-3841, 1971.

Eldholm, O. and M. Talwani, Sediment distribution and structural framework of the Barents Sea. Geological Society of America Bulletin, 88, 1015-1029, 1977.

Eller, A.I., Findings and recommendations of the surface loss model working group: final report, 1984, NORDA technical note 279, NSTL Mississippi, 1-18 + appendices, 1984.

Foster, L.A., Ø.M. Johannessen, and C. Isoppo, Oceanographic summary of the Barents Sea south of Bear Island in the summer, SACLANTCEN Memo. SM-52, SACLANT ASW Res. Centre, La Spezia, Italy, 1974.

Frebold, H., Geologie des Barentsschelfes, Abhandl. Deut. Akad. Wiss. Berlin, 5, 1-150, 1951. (In German)

Gathman, S.G., Climatology, in Nordic Seas, edited by B.G. Hurdle, Springer-Verlag, New York, 1-16, 1986.

Heathershaw, A.D., C.E. Stretch, and S.J. Maskell, Coupled ocean-acoustic model studies of sound propagation through a front, J. Acoustic. Soc. Am., 89 (1), 145-155, 1991.

Helland-Hansen, B., F. Nansen, The Norwegian Sea, Fisk. Dir. Skr.Ser. HavUnders., 2(2), 1-360, 1909.

Houtz, R.E., Preliminary sonobuoy study of rapidly accumulating shelf sediments, J. Geophys. Res., 83, 5397-5404, 1978.

Houtz, R.E., Seafloor and near-surface sound velocities from Barents Sea sonobuoy data., J. Geophys. Res., 85, 4838-4844, 1980.

Houtz, R. and C. Windisch, Barents Sea continental margin sonobuoy data, Geol. Soc. Amer. Bull., 88, 1030-1036, 1977.

Johannessen, Ø.M. and L.A. Foster, A note on the topographically controlled oceanic polar front in the Barents Sea, J. Geophys. Res., 83, 4567-4571, 1978.

Johannessen, Ø.M., Brief overview of the Physical Oceanography, in Nordic Seas, edited by B. G. Hurdle, pp. 110-121, Springer-Verlag, New York, 1986.

Jones, R.M., J.P. Riley and T.M. Georges, HARPO a versitile three-dimensional hamiltonian ray-tracing program for acoustic waves in an ocean with irregular bottom., Wave Prop. Lab. NOAA, Boulder, Colorado, 457 pp.

Katz, S. and M. Ewing, Seismic refraction measurements in the Atlantic Ocean, VII, Geol. Soc. Amer. Bull, 67, 475-510, 1956.

Kinsler, L., A. Frey, A. Coppens, and J. Sanders, Fundamentals of Acoustics, fourth edition, John Wiley & Sons, N.Y., 1982.

Klenova, M.V., Geology of the Barents Sea, U.S. Navy Hydrographic office Translation no. 130, 1-16, Washington, D.C., 1961.

Klenova, M.V., Barents Sea and White Sea, in The Encyclopedia of Oceanography, edited by Fairbridge, R.W., Reinhold Publishing Corp., N.Y., 95-101, 1966.

LePichon, X., J. Ewing, and R. Houtz, Deep sea velocity determination made while reflection profiling, J. Geophys. Res., 73, 2597-2614, 1968.

Loeng, H., Features of the physical oceanographic conditions of the Barents Sea, (In press), 1991.

Loeng, H., Institute of Marine Research, Ministry of Fisheries, Bergen-Nordnes, Norway, Personal Communication, 1991.

Loeng, H., O. Nakken, A. Raknes, The distribution of Copelin in the Barents Sea in relation to water temperature in the period 1974-1982, Fisken Hav., 1983(1), 1-17, 1983 (In Norwegian)

Loeng, H., T. Vinje, On the sea ice conditions in the Greenland and Barents Seas, in POAC 79. Proceedings of the Fifth International Conference on the Port and Ocean Engineering under Arctic Conditions, edited by Anon, 163-174, The Norwegian Institute of Technology, Trondheim, 1979.

Midttun, L., and H. Loeng, Climatic variation in the Barents Sea, in The effects of oceanographic conditions on distribution and population dynamics of commercial fish stocks in the Barents Sea; proceedings of the third Soviet-Norwegian symposium, Murmansk, 26-28 May 1986, edited by H. Loeng, 13-27, Institute of Marine Research, Bergen, 1987.

Midttun, L., Formation of dense bottom water in the Barents Sea, Deep-Sea Research, 32(10), 1233-1241, 1985.

Munk, W. and C. Wunsch, Ocean acoustic tomography: a scheme for large scale monitoring, Deep Sea Res., Part A, 26, 123-161, 1979.

Nansen, F, Northern waters: Captian Roald Amundsen's oceanographic observations in the Arctic Seas in 1901., Skr. Vidensk. Selsk. Christiania Mat.- naturv. Kl., 145 pp., 1906.

NAVOCEANO Publication SP-279-2, U.S. Naval Oceanographic Office, NSTL, Mississippi, 1989.

Newhall, A.E., J.F.Lynch, C.S. Chiu and J.R. Daugherty, Improvements in three-dimensional raytracing codes for under water acoustics, Computational Acoustics, Vol 1, 1987.

Norina, A.M., Hydrological characteristics of the northern Barents Sea, U.S. Naval Oceanographic Office Translation no. 373, 1-27, Washington, D.C., 1968.

Novitskiy, V.P., Permanent currents of the northern Barents Sea., U.S. Naval Oceanographic Office Translation no. 349, 1-32, 1967.

Orsi, T.H. and D.A. Dunn, Correlations between sound velocity and related properties of glacio-marine sediments: Barents Sea, Geo-Marine Letters, In Press, 1991.

Ort, C.M., Spatial and Temporal Variability of Cross-Basin Acoustic Ray Path, M.S. Thesis, Naval Postgraduate School, Monterey, CA., 84pp., 1990.

Parker, R.L., Understanding inverse theory, Ann. Rev. Earth Planet. Sci., 1977.5,35-64, 1977.

Pond, S. and G.L. Pickard, Introductory Dynamical Oceanography 2nd ed., Pergamon Press, New York, 310-311, 1983.

Reynolds, M.F., Department of Oceanography Naval Postgraduate School, Monterey, CA, Personal communication, 1991.

Sach, V.N., and S.A. Strelkov, Mesozoic and Cenozoic of the Soviet Arctic, Geology of the Arctic; Proceedings of the First International Symposium on Arctic Geology, Vol II, ed. by G.O. Raasch, University of Toronto Press, 48-67, 1960.

Sarynina, R.N., Conditions of origin of cold deep-sea waters in the Bear Island channel, Coun. Meet. Int. Counc. Explor. Sea, 1969, (Symp: 28):1-8 (Mimeo), 1969.

Sarynina, R.N., Temperature regime of the water masses in the southern Barents Sea in 1978, Annls. Biol., 35, 62-64, 1980.

Skettering, A. and C.C. Leroy, Sound attenuation between 200Hz and 10kHz, J. Acoust. Soc. Am., vol 69, 276-282, 1971.

Spindel, R.C., Ocean acoustic tomography: a review, Current Practices and New Technology in Ocean Engineering, Vol 11, 7-13, 1986.

Sutton, G. and L. Maynard, Ocean bottom sediment velocity determined from critical range multiple reflections (abstract), EOS Trans. AGU, 52,4, 1971.

Swift, J.H., T.Takahaski and H.D.Livingston, The contribution of the Greenland and Barents Seas to the Deep Water of the Arctic Ocean, J. Geophys. Res., vol 88, no c10, 5981-5986, 1983.

Tolstoy I. and C.S. Clay, Ocean Acoustics, McGraw-Hill, New York, 1966.

Urick, R., Principles of Underwater Sound 3rdEdition, McGraw-Hill, New York, 423, 1983.

Welsh, J.P., R.D. Ketchum, A.W. Lohanick, L.D. Farmer, D.T. Eppler, R.E. Burge and C.J. Radl, A compendium of arctic environmental information, Naval Ocean Research and Development Activity Report-138, NSTL Mississippi, 20-25 + appendix A, 1986.

Wiggins, R.A., The general linear inverse problem: implication of surface waves and free oscillations for earth structures, Reviews of Geophys. and Space Phys., 10, 1, 251-285, 1972.

INITIAL DISTRIBUTION LIST

		No. Copies
1.	Defense Technical Information Center Cameron Station Arlington, VA 22304-6145	2
2.	Library, Code 52 Naval Postgraduate School Monterey, CA 93943-5002	2
3.	Chairman (Code OC/Co) Department of Oceanography Naval Postgraduate School Monterey, CA 93943-5000	1
4.	Library Scripps Institution of Oceanography P.O. Box 2367 La Jolla, CA 92037	1
5.	Professor Ching-Sang Chiu (Code OC/Ci) Department of Oceanography Naval Postgraduate School Monterey, CA 93943-5000	1
6.	Professor James H. Miller (Code EC/Mr) Department of Electrical and Computer Engineering Naval Postgraduate School Monterey, CA 93943-5000	1
7.	Professor Robert Bourke (Code OC/BF) Department of Oceanography Naval Postgraduate School Monterey, CA 93943-5000	1
8.	Professor James F. Lynch Department of Applied Ocean Physics and Engineering Woods Hole Oceanographic Institution Woods Hole, MA 02543	1
9.	Director Naval Oceanography Division Naval Observatory 34th and Massachuetts Avenue NW Washington, DC 20390	1

10. Commander 1
Naval Oceanographic Command
Stennis Space Center
MS 39529-5000

11. Commanding Officer 1
Naval Oceanographic and Atmospheric
Research Laboratory
Stennis Space Center
MS 39529-5004

12. Dr. Thomas Curtin 1
Office of Naval Reasearch
800 North Quincy Street
Arlington, VA 22217-5000

13. Lt. John M. Emblidge USN 1
Naval Submarine School
Code SOAC Class 92010
Groton, CT 06349-5700